JOURNAL OF COMPUTATIONAL PHYSICS **129,** 8–29 (1996)
ARTICLE NO. 0230

The Onset of Instability in Exact Vortex Rings with Swirl

Alexander Lifschitz,*[,1] W. Henry Suters,†[,2] and J. Thomas Beale‡[,2]

*Department of Mathematics, University of Illinois at Chicago, Chicago, Illinois 60607; †Department of Mathematics, Carson-Newman College, Jefferson City, Tennessee 37760; and ‡Department of Mathematics, Duke University, Durham, North Carolina 27708

Received June 9, 1995; revised March 19, 1996

We study the time-dependent behavior of disturbances to inviscid vortex rings with swirl, using two different approaches. One is a linearized stability analysis for short wavelengths, and the other is direct flow simulation by a computational vortex method. We begin with vortex rings which are exact solutions of the Euler equations of inviscid, incompressible fluid flow, axisymmetric, and traveling along the axis; swirl refers to the component of velocity around the axis. Exact vortex rings with swirl can be computed reliably using a variational method. Quantitative predictions can then be made for the maximum growth rates of localized instabilities of small amplitude, using asymptotic analysis as in geometric optics. The predicted growth rates are compared with numerical solutions of the full, time-dependent Euler equations, starting with a small disturbance in an exact ring. These solutions are computed by a Lagrangian method, in which the three-dimensional flow is represented by a collection of vortex elements, moving according to their induced velocity. The computed growth rates are typically found to be about half of the predicted maximum, and the dependence on location and ring parameters qualitatively matches the predictions. The comparison of these two very different methods for estimating the growth of instabilities serves to check the realm of validity of each approach.

1. INTRODUCTION

In this paper we study the time-dependent behavior of disturbances to inviscid vortex rings with swirl, using two different methods. One approach is a linearized stability analysis for short wavelengths. The other is a direct time-dependent simulation using a computational vortex method. The vortex rings of interest are exact solutions of the Euler equations of inviscid, incompressible fluid flow. They are unchanged in time, except for propagation along an axis, and symmetric about the axis; swirl refers to the component of velocity around the axis. Vorticity is confined to a toroidal region. Vortex rings with swirl can be computed numerically using a variational method [11, 12, 38]. A variety of such rings are found here, using an improvement of the method in [12]. Once a ring has been computed, quantitative predictions can be made for the growth rates of certain instabilities, using a novel theory developed recently by Lifschitz and Hameiri [21–24]. They use approximations of WKB type, as in geometric optics, valid for small amplitude, short wavelength disturbances. The predicted growth rates can be compared with numerical solutions of the full, time-dependent Euler equations. We compute solutions of the perturbed problems using a three-dimensional vortex method, in which the flow is represented by a collection of Lagrangian vortex elements, moving according to their induced velocity. The asymptotic analysis and the numerical solution are two very different means for describing the dynamics of the perturbed ring; the comparison of results serves to check the realm of validity of each approach. In addition, the time-dependent simulation of numerically exact solutions of the Euler equations provides a test for the quantitative performance of the vortex method.

Vortex rings are the primary class of steady, inviscid, three-dimensional fluid flow with vorticity of limited extent. The study of instabilities in vortex tubes and rings can be viewed as one route toward the further understanding of inviscid dynamics in fully developed flow. The motion of vortex rings has been studied extensively; see [2, 33] for basic descriptions and [34] for a recent survey. In particular, analysis of linear disturbances to thin rings has explained azimuthal instabilities [25, 32, 39, 40]. Recent numerical computations [18] of vortex rings without swirl, using vortex methods, have compared well with this analysis. Other computations of instabilities, using a difference method for viscous flow, are presented in [35]. Also closely related is a numerical study of axisymmetric jets [26, 27], using vortex methods, showing development of ring-like structures. However, most theory for vortex rings has dealt with perturbations in thin rings without swirl. Here, in contrast, we focus on localized disturbances in *exact* rings with significant structure inside the core, and with a general velocity field including a swirl component. A study similar to this one was done by Bayly [3], for a class of steady solutions to the Euler equations which he called quasi-two-dimensional; they are two-dimensional flows with an added third velocity component. He compared instabilities predicted by short-wave asymptotics with numerical solutions found via a spectral method.

[1] Research supported by NSF Grant No. IRI-9224605.
[2] Research supported by NSF Grant No. DMS-9102782.

0021-9991/96 $18.00

For axisymmetric flow, the presence of a swirl component of velocity has important effects. If there is no swirl, the fluid motion is restricted to cross sections through the axis, and a scalar vorticity is conserved. In this sense, flow without swirl resembles two-dimensional flow. Vortex rings with swirl are thus more representative of general 3D flow than the more familiar rings without. The particle paths in rings without swirl are closed curves within the cross section; for rings with swirl, they are typically helices. Several existence proofs have been given for exact vortex rings without swirl, using somewhat different formulations [13, 14]. With or without swirl, the problem can be written in terms of a stream function for the flow within the cross section. Turkington proved existence of a class of exact rings with swirl [37]. The choice of ring depends on two distribution functions for the core and two parameters. One parameter controls swirl, and connects the familiar case without swirl to the opposite extreme of so-called Beltrami flow, in which the velocity and vorticity fields are parallel. The choice of distribution functions can be made so that the ring is as smooth as desired. Smooth rings are preferable here for the sake of numerical accuracy. A different approach to rings with swirl, due to Moffatt [29, 30], is based on the analogy with magnetohydrodynamics. There are only a few explicit examples of exact solutions, the best known being the Hill spherical vortex. However, as a test problem, it has the disadvantage that the vorticity is discontinuous at the boundary. The Hill vortex is a limiting case of rings without swirl, the opposite of the thin core limit. It is also the extreme case of a family of explicit spherical vortices with swirl; see [28].

The existence theorem of Turkington [37] was based on a variational formulation of the problem. A closely related numerical method for finding solutions was developed by Eydeland and Turkington [11, 12, 38]. A constrained variational problem is discretized and solved iteratively. Since the unknowns are functions of only two variables, they can be computed reliably. The accuracy of the ring obtained numerically is important for the present study. In [12], a truncated domain was used, and the artificial boundary introduces errors. In the present work, the far-field boundary condition is imposed more carefully, by exact computation of the free space solution at the artificial boundary. This permits better resolution, since the boundary need not be far away from the vortex core. The family of rings studied here and the numerical method used to compute them are described in detail in Section 2.

Lifschitz and Hameiri [21–24] have developed a general theory of localized instabilities in inviscid fluid flow, using perturbations in a small parameter, representing short wavelength, as in geometric optics. The disturbance is described by a system of ordinary differential equations for the wave vector and amplitude, along particle paths in the underlying flow, with coefficients depending on the unperturbed velocity field. The application of this theory to vortex rings is summarized in Section 3. After a ring has been computed using the method described above, the ordinary differential equations for the localized disturbances are known numerically and can be solved numerically. Their solution leads to a prediction of growth rates, which are defined in a precise way in Section 3, for comparison with numerical solutions of the Euler equations.

For the computation of time-dependent solutions of the Euler equations, we use a three-dimensional vortex method. Such methods have been used for some time [8, 9, 19, 20]. There are several versions, but all are closely related; see [17, 31] for recent surveys and [5, 6, 18, 26, 27, 41] for other applications. Here we compute paths of a collection of representative particles in the fluid and the values of the vorticity vector at their locations. The velocity of the particles is determined by the Biot–Savart Law, and the vorticity is stretched by the gradient of velocity. The specific formulation is given in Section 4. This version of the vortex method was introduced in [1]; it was proved in [4, 10] that it converges to exact solutions of the Euler equations. Earlier theory is summarized in [6]. This method is well suited for the computation of disturbances in vortex rings, since the vorticity remains in a bounded region, and no artificial boundary is needed. The computational elements follow the transport of vorticity. Several modifications of this method are used here, however. When a perturbation of a steady flow is computed, it is possible to subtract out the underlying exact solution, without introducing new errors, so that the accumulation of error from recomputing it at each time step can be avoided. This modification is explained in Section 4. To reduce the expense of the summation in the Biot–Savart Law, we use a fast summation method of the type developed by Greengard and Rokhlin [15, 16]; the version we use here is due to Buttke [7]. We also assume fourfold rotational symmetry in order to reduce the computation.

In Section 4 we carry out time-dependent computations of vortex rings using the vortex method, without introducing a perturbation. A ring computed as a steady solution by the variational method is used as an initial state on a regular mesh. The deviation of the ring at later time from its initial state is entirely due to the error in computing the initial ring and the error of the time-dependent numerical scheme, interacting with the instabilities of the ring itself. These calculations are made to build confidence that the computation is not seriously dependent on the mesh size and that certain of the rings are stable enough that they maintain their shape for a reasonable length of time in the calculation. A similar test with one ring was reported earlier in [5]; however, it was not well enough resolved initially, and it appears to be less stable than other rings chosen here. The vortex method computations of these rings are typically more accurate than the example in [5].

Section 4 includes computations with a regridding scheme; after a number of time steps, new particles are introduced on a regular mesh, and the vorticity is redistributed. It is found that the growth of error can be reduced significantly in this manner.

In Section 5 we study the growth of perturbations in vortex rings using the modified version of the vortex method described above. We begin with a numerically exact ring and add a disturbance localized to the core of the ring, but which is otherwise not chosen in a special way. The disturbance is then computed at a later time. Growth rates are obtained for a variety of rings and compared with the predictions from the analytical theory. Several different rings are considered. In all cases but one, the observed growth rates are about $\frac{1}{3}$ to $\frac{1}{2}$ of the predicted maximum. The observed dependence on location and on the parameters in the rings generally matches qualitatively that of the predictions. The short-wave asymptotic analysis neglects interactions between different regions and nonlinear effects; the vortex method calculation accounts for these, but introduces numerical errors. For the two to be in reasonable agreement, both types of errors must be subordinate to the instability being sought. Further interpretation of the results is given in Section 5 and in the Conclusions.

Preliminary versions of these results were reported in the Ph.D. thesis of Suters [36]. We are especially grateful to T. Buttke and B. Turkington for their help and suggestions.

2. STEADY VORTEX RINGS WITH SWIRL

To evaluate the performance of numerical methods for solving the Euler equations, as well as to understand the development of fully nonlinear effects, it is desirable to have analytical solutions for direct comparison. In general, however, it is extremely difficult to find exact nontrivial solutions to the Euler equations in free space. In order to make time-dependent numerical simulation feasible, it is also desirable to have solutions with compactly supported, smooth vorticity. It is in fact possible to find such solutions, up to reliable computation, by reducing the number of independent variables. Whereas the full Euler equations depend on three space variables and time, we seek solutions which reduce to two independent variables. These special solutions are assumed to be independent of time except for translation. Furthermore, they are assumed to be axisymmetric, thereby eliminating one spatial variable. The primary examples of solutions with these special properties are vortex rings.

Vortex rings are best represented in cylindrical coordinates (r, θ, z), where the z-axis is the axis of symmetry. In this coordinate system the axisymmetry of the ring implies that both the velocity and vorticity fields are functions of (r, z). While the velocity field is not compactly supported, the vorticity field is confined to a toroidal region about the z-axis, the vortex core. Vortex rings are steady solutions of the Euler equations, except for translation along the z-axis. The most common physical example of a vortex ring is a smoke ring. In this paper we are concerned with vortex rings which have a thick cross section and significant internal structure. Much previous study of vortex rings has used a model in which the ring is thin, or close to a single vortex filament [2, 18, 25, 32–34,39, 40].

The θ-component of the velocity is called the swirl velocity. The qualitative behavior of the flow is quite different, depending on whether or not swirl is present. In vortex rings without swirl, for which the θ-component is identically zero, the particles in the flow are confined to azimuthal cross sections of the ring. Thus, the particles move along two-dimensional paths, and the flow has many of the characteristics associated with two-dimensional problems. These rings without swirl have been studied extensively ([13, 14, 35], as well as the above) and there is considerable information about their behavior and stability characteristics. Less well known and studied are vortex rings where the θ-component is not identically zero. These rings are not commonly observed in nature but they do have a more typically three-dimensional behavior. Particles move in helices within the vortex core. For these reasons, vortex rings with swirl may make better test problems for studying the performance of three-dimensional numerical methods. There has not been much research into understanding the behavior and stability of these rings, however. It has even been suggested that rings with swirl are not commonly observed because they are much less stable than those without.

The analysis of vortex rings with swirl can be reduced to studying a scalar semi-linear elliptic equation for the Stokes stream function ψ (see below). The actual form of the equilibrium equation depends on two arbitrary structure functions of ψ. Solving this equation is difficult for two reasons. First, the location of the free vortex core boundary is not known a priori. Second, the equation has to be solved in the entire half-space. The equilibrium problem was studied by Turkington [37] via a variational technique. (Another point of view was given in [29, 30].) It was proven in [37] that a wide variety of vortex rings with swirl can be constructed with choices of certain core functions. Further, the method of proof was extended to a numerical method for generating these rings in [12]; see also [11, 38].

The numerical method in [12] treats the free-boundary aspect of the problem in an adequate way. However, it deals with the boundary conditions at infinity in a less successful manner by replacing the problem in the entire space by the problem in a finite computational domain with a simple choice of boundary conditions. To avoid the interference of the boundary with the solution inside the vortex core, the size of the computational domain and the

number of grid points have to be made very large, so that an accurate description of the vorticity field becomes prohibitively expensive. In the present paper we develop a different approach to the free-space aspect of the problem. Namely, we introduce a finite computational domain containing the vorticity core and impose nonreflective conditions on its boundary. These conditions guarantee that the stream function inside the computational domain can be smoothly matched with the stream function outside this domain. This approach allows us to deal with computational domains just slightly larger than the core and to resolve the fine features of the vorticity field with very high accuracy. To be specific, we consider the polynomial structure functions of ψ depending an a finite number of parameters. Our numerical method converges to exact solutions of the Euler equations and generates a multi-parameter family of rings. This section is devoted to explaining the development of this numerical scheme. The characteristics of the rings controlled by each of the parameters are also discussed.

We regard the vortex rings as special solutions of the Euler equations of inviscid, incompressible flow

$$\frac{\partial \mathbf{u}}{\partial t} + \mathbf{u} \cdot \nabla \mathbf{u} = -\nabla p \tag{1}$$

$$\nabla \cdot \mathbf{u} = 0,$$

where $\mathbf{u}$ is the velocity and p is the pressure. We first write the Euler equations for time-independent flow in modified cylindrical coordinates (y, θ, z), with $y = r^2/2$, and in a form which exploits the axisymmetry of the solutions we wish to find. The equations are

$$\mathbf{u} \cdot \nabla u^y - \frac{1}{\sqrt{2y}} (u^\theta)^2 = -\sqrt{2y} p_y, \tag{2}$$

$$\mathbf{u} \cdot \nabla u^\theta + \frac{1}{\sqrt{2y}} u^y u^\theta = 0, \tag{3}$$

$$\mathbf{u} \cdot \nabla u^z = -p_z, \tag{4}$$

$$(\sqrt{2y} u^y)_y + u^z_z = 0. \tag{5}$$

Here

$$\mathbf{u} = u^y(y, z)\hat{e}_y + u^\theta(y, z)\hat{e}_\theta + u^z(y, z)\hat{e}_z,$$

where $\hat{e}_y$, $\hat{e}_\theta$, $\hat{e}_z$ are the orthonormal basis vectors in the cylindrical coordinate system, $p = p(y, z)$, and

$$\mathbf{u} \cdot \nabla = \sqrt{2y} u^y \, \partial/\partial y + u^z \, \partial/\partial z$$

because of axisymmetry. The corresponding vorticity can be written as

$$\boldsymbol{\omega} = \nabla \times \mathbf{u} = -u^\theta_z \hat{e}_y + (u^y_z - \sqrt{2y} u^z_y)\, \hat{e}_\theta + (\sqrt{2y} u^\theta)_y \hat{e}_z.$$

The incompressibility equation (5) implies that there is a Stokes stream function $\psi = \psi(y, z)$ such that

$$\mathbf{u} = -\frac{1}{\sqrt{2y}} \psi_z \hat{e}_y + u^\theta \hat{e}_\theta + \psi_y \hat{e}_z, \tag{6}$$

$$\boldsymbol{\omega} = -u^\theta_z \hat{e}_y - \frac{1}{\sqrt{2y}} \mathscr{L}\psi \hat{e}_\theta + (\sqrt{2y} u^\theta)_y \hat{e}_z,$$

where $\mathscr{L}$ is the linear elliptic operator

$$\mathscr{L} = 2y \frac{\partial^2}{\partial y^2} + \frac{\partial^2}{\partial z^2}. \tag{7}$$

By manipulating Eqs. (4), (2), (3) we obtain the following equations for u^θ and ω^θ

$$\mathbf{u} \cdot \nabla(\sqrt{2y} u^\theta) = 0, \tag{8}$$

$$\mathbf{u} \cdot \nabla \left(\frac{1}{\sqrt{2y}} \omega^\theta \right) - \frac{1}{2y} ((u^\theta)^2)_z = 0 \tag{9}$$

and conclude that

$$u^\theta = \frac{1}{\sqrt{2y}} f(\psi), \quad \omega^\theta = -\sqrt{2y} h'(\psi) + \frac{1}{\sqrt{2y}} f(\psi) f'(\psi). \tag{10}$$

Here f and h are *arbitrary* functions of ψ, and $f' = df/d\psi$, $h' = dh/d\psi$. Physically they represent the circulation around circles centered at the axis of symmetry and the Bernoulli head function, respectively. The equilibrium equation for ψ can be written as

$$\mathscr{L}\psi = 2y h'(\psi) - f(\psi) f'(\psi). \tag{11}$$

We impose the following boundary conditions on ψ (cf. [37])

$$\psi = -\mu \text{ on } y = 0, \quad \psi \to -(\mu + \nu y) \text{ as } |(y, z)| \to \infty. \tag{12}$$

Recall that we are attempting to find a steady solution with compactly supported vorticity which is embedded in the uniform flow. Suppose that the support of the vorticity cross section is a connected compact subset Ω of $\Re^2_+$. It is clear that ψ is constant on the boundary of Ω, and it will suffice to consider f and h such that $f = 0$, $h = h_0 > 0$ outside Ω.

At this stage it is convenient to introduce the adjusted stream function $\tilde{\psi} = \psi + \mu + \nu y$ and to rewrite the equilibrium equation and the boundary conditions in the form

$$\mathscr{L}\tilde{\psi} = 2yh'(\tilde{\psi} - \mu - \nu y) - f(\tilde{\psi} - \mu - \nu y)f'(\tilde{\psi} - \mu - \nu y), \tag{13}$$

$$\tilde{\psi} = 0 \text{ on } y = 0 \quad \tilde{\psi} \to 0 \text{ as } |(y, z)| \to \infty. \tag{14}$$

The constants μ and ν play an important role in the definition of $\tilde{\psi}$. They represent the constant value of ψ on the axis of symmetry and the uniform axial velocity at infinity, respectively. It is clear that the adjusted stream function $\tilde{\psi}$ is associated with the vorticity localized in the vortex core Ω. We need two additional conditions to determine the values of μ and ν. These conditions take the form of conserved quantities of axisymmetric flows given by

$$-\int\int \frac{1}{y}(2yh' - ff')\, dy\, dz = C, \tag{15}$$

$$-\int\int (2yh' - ff')\, dy\, dz = P. \tag{16}$$

In the standard interpretation of these quantities C corresponds to meridional circulation and P corresponds to the axial component of linear impulse.

We choose the structure functions f and h to be

$$f(\psi) = \sqrt{2\alpha/(\zeta + 1)}\, \psi_+^{(\zeta+1)/2}, \tag{17}$$

$$h(\psi) = h_0 - \frac{\beta}{2(\zeta + 1)}\, \psi_+^{\zeta+1},$$

where $\psi_+ = \max(\psi, 0)$, and $h_0, \alpha, \beta, \zeta$ are arbitrary positive constants. (The value of h_0 is irrelevant.) The values of the positive conserved quantities C and P can be controlled by the way in which the problem is nondimensionalized. By stretching the variables and the coefficients according to the rule

$$y \to \frac{P}{C}\, y, \quad z \to \frac{P^{1/2}}{C^{1/2}}\, z, \quad \psi \to \frac{C^{3/2\zeta}}{P^{1/2\zeta}}\, \psi,$$

$$\alpha \to \alpha, \quad \beta \to \frac{C}{P}\, \beta, \quad \mu \to \frac{C^{3/2\zeta}}{P^{1/2\zeta}}\, \mu, \quad \nu \to \frac{C^{3/2\zeta+1}}{P^{1/2\zeta+1}}\, \nu,$$

we can normalize these quantities to unity and assume that $C = 1$ and $P = 1$. This normalization guarantees that the linear size of the vorticity core is of order unity.

The equilibrium problem then reduces to the equation

$$\mathscr{L}\tilde{\psi} = -(\alpha + \beta y)(\tilde{\psi} - \mu - \nu y)_+^{\zeta}, \tag{18}$$

subject to the constraints

$$\int\int \frac{1}{y}(\alpha + \beta y)(\tilde{\psi} - \mu - \nu y)_+^{\zeta}\, dy\, dz = 1, \tag{19}$$

$$\int\int (\alpha + \beta y)(\tilde{\psi} - \mu - \nu y)_+^{\zeta}\, dy\, dz = 1, \tag{20}$$

and the homogeneous boundary conditions (14). The quantities to be determined are the adjusted stream function $\tilde{\psi}$ and the constants μ, ν. A proof that a solution to this problem in the half-plane exists is presented in [37] and the proof is extended in [12] to produce a convergent numerical method for solving the problem (18), (19), (20) in a a finite computational domain $R = \{(y, z) | 0 \le y \le Y, -Z \le z \le Z\}$ with the mixed Dirichlet–Neumann boundary conditions

$$\tilde{\psi}_z(y, \pm Z) = 0, \quad \tilde{\psi}(0, z) = 0, \quad \tilde{\psi}(Y, z) = 0. \tag{21}$$

It is assumed that the linear size of the domain R is so large that the presence of the boundary does not affect the solution inside the vorticity core in a noticeable way. The proof and numerical method are both based on a variational approach. The authors show that the solutions are extreme points of a modified energy functional and that such extrema exist; they also provide an iterative approach for finding the extreme points.

In our approach a reduction of the problem in the half-space to a problem in a finite computational domain R also plays a prominent role. However, boundary conditions (21) are replaced by the following nonreflective (and nonlocal) conditions on the boundary of R,

$$\tilde{\psi}(y, \pm Z) = \phi(y, \pm Z), \quad \tilde{\psi}(0, z) = 0, \quad \tilde{\psi}(Y, z) = \phi(Y, z), \tag{22}$$

where

$$\phi(y, z) = -\int\int \mathscr{G}(y, \bar{y}, z, \bar{z})(\alpha + \beta\bar{y})(\tilde{\psi} - \mu - \nu\bar{y})_+^{\zeta}\, d\bar{y}\, d\bar{z}. \tag{23}$$

Here $\mathscr{G}$ is the Green's function for the operator $\mathscr{L}$ in the free space,

$$\mathscr{G}(y, \bar{y}, z, \bar{z}) = -\frac{1}{2\pi}\frac{(2y)^{1/4}}{(2\bar{y})^{3/4}}\left[\left(\frac{2}{k} - k\right)K(k) - \frac{2}{k}E(k)\right], \tag{24}$$

where $K(k)$ and $E(k)$ are the complete elliptic integrals of the first and second kind of modulus k, and

$$k^2 = \frac{4(2y)^{1/2}(2\bar{y})^{1/2}}{((2y)^{1/2} + (2\bar{y})^{1/2})^2 + (z - \bar{z})^2}.$$

Thus ϕ represents the exact solution on the computational boundary of the half-space problem for $\tilde{\psi}$. These conditions guarantee that the stream functions inside the computational domain can be smoothly extended to infinity. This allows us to consider a much smaller computational domain, provided that it contains the vorticity core. This

is a crucial step towards improving the accuracy of the numerical method.

Following [37, 12] we solve the problem (18), (19), (20), (22) by iteration. An iteration step can be described as follows. Suppose that the triple $\tilde{\psi}^{(n)}$, $\mu^{(n)}$, $\nu^{(n)}$ is known. First, we use this triple to compute

$$\chi^{(n)} = -(\alpha + \beta y)(\tilde{\psi}^{(n)} - \mu^{(n)} - \nu^{(n)} y)_+^{\zeta} \tag{25}$$

and to find the corresponding $\phi^{(n)}$ via the relation

$$\phi^{(n)} = \int\int \mathcal{G}\chi^{(n)}\, dy\, dz. \tag{26}$$

Second, we determine $\tilde{\psi}^{(n+1)}$ from the following boundary value problem:

$$\mathcal{L}\tilde{\psi}^{(n+1)} = \chi^{(n)} \text{ in } R; \quad \tilde{\psi}^{(n+1)} = \phi^{(n)} \text{ on } \partial R. \tag{27}$$

Finally, we determine $\mu^{(n+1)}$, $\nu^{(n+1)}$ from the conditions

$$\mathcal{C}(\mu^{(n+1)}, \nu^{(n+1)}) = \int\int \frac{1}{y}(\alpha + \beta y)(\tilde{\psi}^{(n+1)} - \mu^{(n+1)} - \nu^{(n+1)} y)_+^{\zeta}\, dy\, dz = 1, \tag{28}$$

$$\mathcal{P}(\mu^{(n+1)}, \nu^{(n+1)}) = \int\int (\alpha + \beta y)(\tilde{\psi}^{(n+1)} - \mu^{(n+1)} - \nu^{(n+1)} y)_+^{\zeta}\, dy\, dz = 1. \tag{29}$$

This part requires solving an implicit system of two algebraic equations with two unknowns μ, ν. This is done via Newton's method. Once the triple $\tilde{\psi}^{(n+1)}$, $\mu^{(n+1)}$, $\nu^{(n+1)}$ is found the iteration step can be repeated until the convergence is reached. The iteration procedure is initiated by choosing a (fairly arbitrary) $\chi^{(0)}$ satisfying the constraints of the form

$$-\int\int \frac{1}{y}\chi^{(0)}\, dy\, dz = 1, \quad -\int\int \chi^{(0)}\, dy\, dz = 1. \tag{30}$$

The method discussed in this section can be used to generate vortex rings with a wide variety of characteristics. We have three parameters, α, β, and ζ, at our disposal. The parameter ζ is mainly used to control the smoothness of the stream function ψ on the boundary of Ω. In general, the stream function ψ is a $C^{\zeta+2}$ function, so that larger values of ζ produce smoother stream functions. In principle, it is desirable to make ψ as smooth as possible because the numerical method that we will use is not designed to deal with singularities. In practice, however, requiring too much smoothness and increasing the value of ζ results in a stream function with a very shallow maximum and a vortex ring which is highly unstable. A particular example of this can be seen in [5], where an exceptionally unstable ring, with $\zeta = 3$, was used as a test problem. Setting $\zeta = 1.5$ seems to be a reasonable compromise. Unless otherwise noted, this is the value which we will use for ζ. Using a fixed value for ζ leaves us with a two parameter family of vortex rings. These parameters are α and β; they control the energy and swirl of the ring.

From Eq. (17), setting $\alpha = 0$ produces a ring where f is identically zero. Since f is the modified θ-component of velocity, this produces a ring without swirl. Thus, vortex rings without swirl arise as a special case of the method discussed here. One of their special characteristics is that the velocity and vorticity are perpendicular. On the other hand, setting $\beta = 0$, produces rings which have parallel velocity and vorticity. To see this note that if $\beta = 0$ then Eqs. (6) produce

$$\boldsymbol{\omega} = \sqrt{\alpha(\zeta + 1)/2}\, \psi_+^{(\zeta-1)/2}\, \mathbf{u}.$$

Thus, $\boldsymbol{\omega}$ is $\mathbf{u}$ times a function of ψ_+. Flows of this special type are known as Beltrami flows. This extreme case represents the maximum amount of swirl which can be present in a steady flow.

To illustrate how the method works, we compute the stream function ψ for a Beltrami vortex ring where $\alpha = 50$, $\beta = 0$, and $\zeta = 1.5$. The values of the stream function ψ are obtained on a 300×300 grid in the yz-coordinate system. Figure 1 is a picture of level curves of ψ in the cross section of the vortex ring in question. The ring is plotted in the yz-coordinate system with z varying from -0.8 to 0.8 and y varying from 0.2 to 2.2. The maximum of ψ is located at the center of the ring and has the value 0.10236. The stream function ψ has the value 0 on the outer loop. The intermediate loops are evenly spaced in terms of ψ.

Once the stream function ψ has been computed it is possible to determine the velocity and vorticity fields using Eqs. (6). Additional information about the structure of the rings can also be obtained. For example the period for each particle to complete a closed path in the azimuthal cross section of the vortex ring can be determined. This period is shown in Fig. 2 for the Beltrami ring. This stream function data can also be used to predict the instability of vortex rings to perturbations with short wavelengths and small amplitudes. These predictions are the topic of Section 3.

3. LOCAL INSTABILITIES

In this section we discuss the stability of general vortex rings using a WKB-type method developed by Lifschitz and Hameiri [21–24], valid for short wavelengths and small amplitude perturbations. We explain a procedure for making quantitative predictions of growth rates. In Section 5

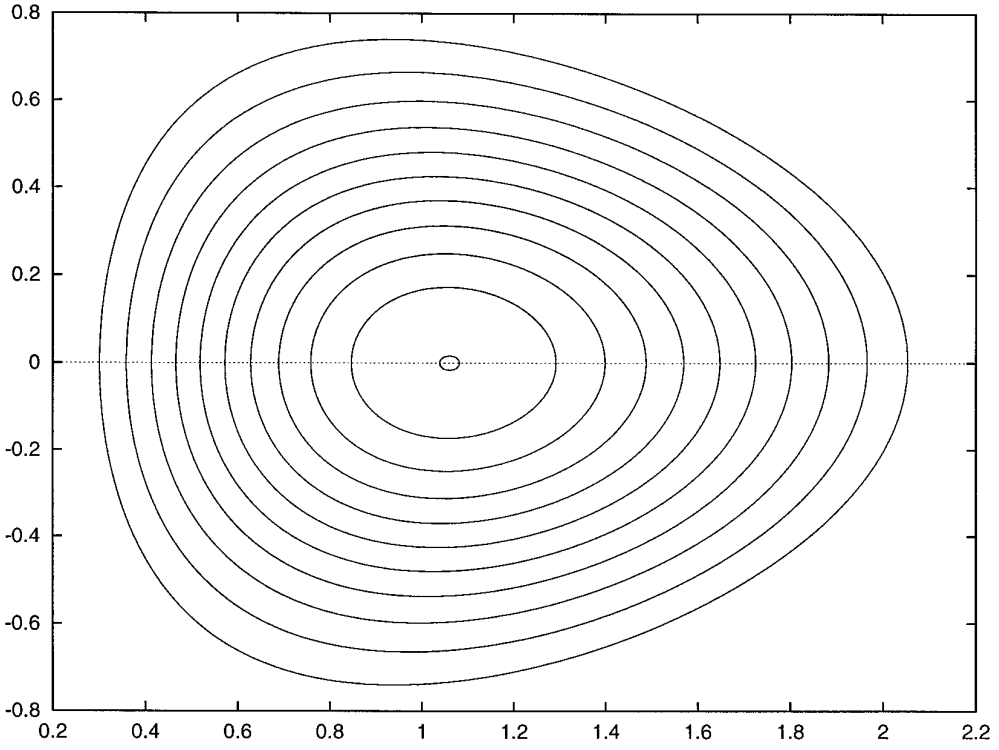

FIG. 1. Vortex ring cross section.

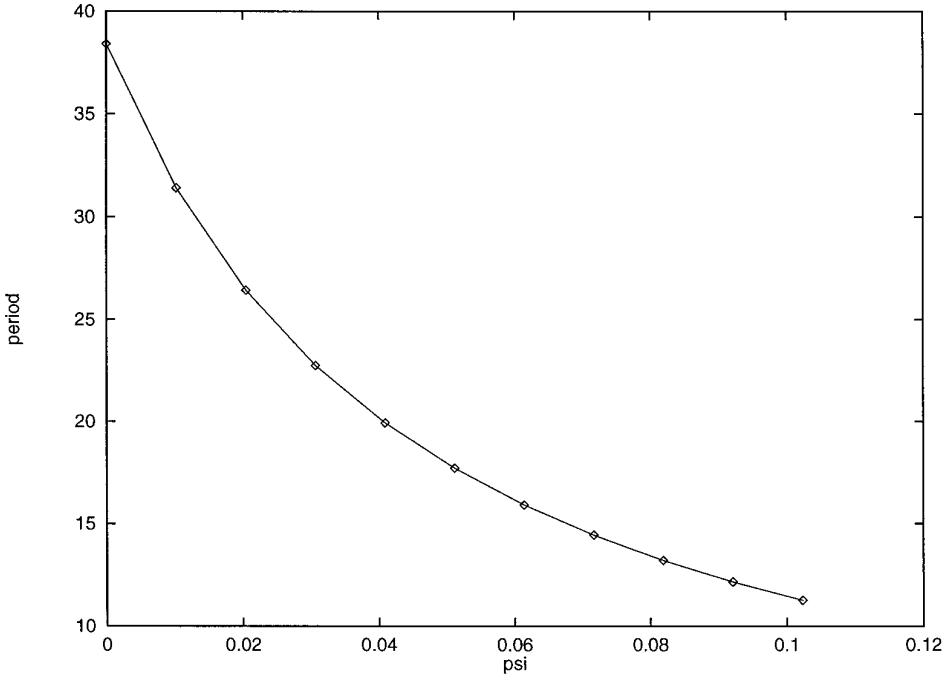

FIG. 2. Azimuthal cross section period.

FIG. 3. A typical vortex ring with swirl. Spiral stream lines winding around stream surfaces are clearly visible. Produced in The Laboratory for Advanced Computing at The University of Illinois at Chicago by R. Grossman, J. Leigh, and A. Lifschitz.

we compute the time-dependent behavior of perturbations to vortex rings using a numerical method to be introduced in Section 4. Comparing the growth of these perturbations with the predicted growth rates enables us to check the validity of the analytical predictions against perturbations with longer wavelengths and larger amplitudes. The stability question is related to an evaluation of the performance of the vortex method or other numerical methods for the time-dependent solution. Indeed, since we can only specify the initial data approximately, the numerical solution departs from the exact solution immediately, and thus the stability of the rings, i.e., the dynamics of solutions initially close to the exact steady state, is an essential issue.

Although little is yet known about the stability properties of vortex rings with swirl (see Fig. 3), there has been extensive research on instabilities in rings without swirl, including [18, 25, 32, 35, 39, 40]. For a review, see [34]. Most theoretical study has been in the limit of thin cores. Linear analysis in this limit leads to predictions of azimuthal instabilities, or wavy modes around the ring [32, 39, 40]. The wave number of the most unstable mode depends on the ring speed, as well as the core distribution. Good agreement was found by Saffman [32] between such predictions and experiments with care given to the core structure. Knio and Ghoniem [18] performed time-dependent simulations of vortex rings without swirl, using a vortex method similar to the one used here, and observed the most unstable modes with various choices of core size and speeds. When several vortex elements were used within the core, their results compared well with the analytical predictions of most unstable modes in [39].

The WKB-type predictions are based on the fact that short wavelength instabilities can be described in terms of the evolution of localized wave envelopes. These envelopes move along with the particles in the fluid flow, and their behavior is governed by a system of characteristic equations along particle trajectories. This system consists of an eikonal equation for the wave vector and transport equation for the velocity amplitude. We determine the stability properties of the flow by determining solutions to a system of ordinary differential equations.

Consider the Euler equations (1) when a steady solution with velocity $\mathbf{u}_s$ and pressure p_s, in our case a vortex ring, are perturbed by a short wavelength, small amplitude perturbation $\mathbf{u}$, p, where $\mathbf{u}$, p evolve in time. Since we are examining the behavior of vortex rings, we can assume that both the velocity $\mathbf{u}$ and pressure p vanish at infinity. We also assume that the perturbation $\mathbf{u}$ begins at time 0 as a short wavelength envelope.

The linearized Euler equations for $\mathbf{u}$, p have the form

$$\frac{D\mathbf{u}}{Dt} + \mathbf{u} \cdot \nabla \mathbf{u}_s + \nabla p = 0, \tag{31}$$

$$\nabla \cdot \mathbf{u} = 0, \tag{32}$$

where

$$\frac{D\mathbf{u}}{Dt} = \frac{\partial \mathbf{u}}{\partial t} + \mathbf{u}_s \cdot \nabla \mathbf{u}$$

is the material derivative and

$$\mathbf{u}(0, \mathbf{x}) = \mathbf{u}_0(\mathbf{x}) \tag{33}$$

is the initial condition. The ring is called linearly stable in the L_2-norm (energy norm) if the relative kinetic energy of the solution is *uniformly* bounded in time, i.e.,

$$\frac{\frac{1}{2}\int |\mathbf{u}(t, \mathbf{x})|^2 \, d\mathbf{x}}{\frac{1}{2}\int |\mathbf{u}_0(\mathbf{x})|^2 \, d\mathbf{x}} < C, \tag{34}$$

where C is a constant independent on t and u_0, otherwise it is called unstable. This definition is essentially due to Lyapunoff. Instabilities captured by this definition can be both exponential and algebraic.

For the general initial data $\mathbf{u}_0$ it is not possible to find the solution $\mathbf{u}(t)$ analytically. However, it is shown in [21] that for the initial data in the form of a short wavelength envelope,

$$\mathbf{u}_0(\mathbf{x}) = \mathbf{a}_0(\mathbf{x}) \exp\left(\frac{i\Phi_0(\mathbf{x})}{\varepsilon}\right), \tag{35}$$

where ε is a small parameter, Φ_0 is the initial phase function, $\mathbf{a}_0(\mathbf{x})$ is the initial amplitude, and $\mathbf{x}$ is the position vector, the corresponding solution can be written in the geometrical optics form as

$$\mathbf{u} = \mathbf{u}_1(t,\mathbf{x}) \exp\left(\frac{i\Phi(t,\mathbf{x})}{\varepsilon}\right) + \varepsilon \mathbf{u}_2(t,\mathbf{x}) \exp\left(\frac{i\Phi(t,\mathbf{x})}{\varepsilon}\right) + O(\varepsilon^2),$$

$$p = p_1(t,\mathbf{x}) \exp\left(\frac{i\Phi(t,\mathbf{x})}{\varepsilon}\right) + \varepsilon p_2(t,\mathbf{x}) \exp\left(\frac{i\Phi(t,\mathbf{x})}{\varepsilon}\right) + O(\varepsilon^2), \tag{36}$$

where $\mathbf{u}_1(t, \mathbf{x})$ is the first-order amplitude and $\Phi(t, \mathbf{x})$ is the wave vector. The initial conditions for these quantities are $\mathbf{u}_1(0, \mathbf{x}) = \mathbf{a}_0(\mathbf{x})$ and $\Phi(0, \mathbf{x}) = \Phi_0(\mathbf{x})$. It is shown in [21] that the leading order term dominates the solution for a sufficiently long time, provided that ε is small enough. Thus, for the purpose of the stability analysis it is sufficient to determine the growth rate of the first-order amplitude.

The eikonal and transport equation describing the dynamics of the phase Φ and the amplitude $\mathbf{u}_1$ are derived in [21]. These equations have the form

$$\frac{D\Phi}{Dt} = 0, \tag{37}$$

$$\frac{D\mathbf{u}_1}{Dt} = -\mathbf{u}_1 \cdot \nabla \mathbf{u}_s + 2\frac{\mathbf{u}_1 \cdot \nabla \mathbf{u}_s \cdot \nabla\Phi}{|\nabla\Phi|^2}\nabla\Phi, \tag{38}$$

with the initial conditions

$$\mathbf{u}_1(0,\mathbf{x}) = \mathbf{a}_0(\mathbf{x}), \quad \Phi(0,\mathbf{x}) = \Phi_0(\mathbf{x}). \tag{39}$$

Note that the eikonal equation for the phase Φ of the flow expresses the fact that waves in an incompressible fluid must travel with the flow. The incompressibility condition (32) implies that $\nabla\Phi$ and $\mathbf{u}_1$ are mutually orthogonal:

$$\mathbf{u}_1 \cdot \nabla\Phi = 0. \tag{40}$$

Our goal here is to determine a growth rate for the first-order amplitude $\mathbf{u}_1$. To do this, we write a system of evolution equations for $\mathbf{x}$, $\nabla\Phi$, and $\mathbf{a}$ from the perspective of a particular particle moving with the flow. This allows us to determine the instability of the flow along the path of that particle. We localize the problem near $\mathbf{x}_p$, a particular particle location, moving with the flow. We define $\mathbf{a}(t) = \mathbf{u}_1(t, \mathbf{x}_p)$, $\mathbf{k}(t) = \nabla\Phi(t, \mathbf{x}_p)$ and obtain the following system of characteristic ordinary differential equations

$$\frac{d\mathbf{x}}{dt} = \mathbf{u}_s, \tag{41}$$

$$\frac{d\mathbf{k}}{dt} = -\nabla\mathbf{u}_s \cdot \mathbf{k}, \tag{42}$$

$$\frac{d\mathbf{a}}{dt} = -\mathbf{a} \cdot \nabla\mathbf{u}_s + 2\frac{\mathbf{a} \cdot \nabla\mathbf{u}_s \cdot \mathbf{k}}{|\mathbf{k}|^2}\mathbf{k}, \tag{43}$$

with the initial conditions

$$\mathbf{x}(0) = \mathbf{x}_0, \quad \mathbf{k}(0) = \nabla\Phi_0(\mathbf{x}_0) = \mathbf{k}_0, \quad \mathbf{a}(0) = \mathbf{a}_0(\mathbf{x}_0). \tag{44}$$

We now have our evolution equations for $\mathbf{x}$, $\mathbf{k}$, and $\mathbf{a}$. These equations consist of the trajectory equation (41) for $\mathbf{x}$, the eikonal equation (42) for $\mathbf{k}$, and the transport equation (43) for $\mathbf{a}$. The first equation determines the stream line passing through $\mathbf{x}_0$. The second determines the evolution of the local wave vector $\mathbf{k}$ along this stream line, and the final equation determines the evolution of the amplitude $\mathbf{a}$, also along this stream line. The system of characteristic equations has a ''triangular'' structure in the following sense. The trajectory depends only on $\mathbf{x}_0$; the wave vector depends on both $\mathbf{x}_0$ and $\mathbf{k}_0$; and finally, the amplitude depends on $\mathbf{x}_0$, $\mathbf{k}_0$, and $\mathbf{a}_0$. The incompressibility condition (40) assumes the form

$$\mathbf{a} \cdot \mathbf{k} = 0. \tag{45}$$

We emphasize that the scalar product $\mathbf{a} \cdot \mathbf{k}$ is conserved by the characteristic equations, so that these equations are compatible with the incompressibility condition, provided that it is satisfied at the initial moment, i.e., $\mathbf{a}_0 \cdot \mathbf{k}_0 = 0$.

The following sufficient instability condition is obtained by Lifschitz and Hameiri [24]: The vortex ring $\mathbf{u}_s$, p_s is unstable in the L_2-norm if for certain initial data $\mathbf{x}_0$, $\mathbf{k}_0$, $\mathbf{a}_0$ such that $\mathbf{a}_0 \cdot \mathbf{k} = 0$ the corresponding amplitude $\mathbf{a}(t)$ grows in time without a bound. We can analyze the stability of a given flow by numerically solving the system of ordinary differential equations (41), (42), (43) along stream lines of this flow.

In the core of a vortex ring, stream lines are confined to level sets of the stream function ψ. Thus, it is possible to calculate numerically a growth rate for $\mathbf{a}$ on each level set of ψ. For a vortex ring characterized by a stream function $\psi(y, z)$ and the profile functions $f(\psi)$, $h(\psi)$, the characteristic equations for $\mathbf{x}$ and the physical components of $\mathbf{k}$, $\mathbf{a}$ can be written as

$$\frac{dy}{dt} = -\psi_z, \quad \frac{d\theta}{dt} = \frac{f(\psi)}{2y}, \quad \frac{dz}{dt} = \psi_y, \tag{46}$$

$$\frac{d}{dt}\begin{pmatrix} k^y \\ k^\theta \\ k^z \end{pmatrix} = \begin{pmatrix} \psi_{yz} - \dfrac{\psi_z}{2y} & -f'\psi_y + \dfrac{f}{y} & -\sqrt{2y}\psi_{yy} \\ 0 & \dfrac{\psi_z}{2y} & 0 \\ \dfrac{\psi_{zz}}{\sqrt{2y}} & -\dfrac{f'\psi_z}{\sqrt{2y}} & -\psi_{yz} \end{pmatrix}\begin{pmatrix} k^y \\ k^\theta \\ k^z \end{pmatrix}, \quad (47)$$

$$\frac{d}{dt}\begin{pmatrix} a^y \\ a^\theta \\ a^z \end{pmatrix} = (\mathscr{I} - 2\mathscr{P}_{\mathbf{k}})\begin{pmatrix} \psi_{yz} - \dfrac{\psi_z}{2y} & \dfrac{f}{2y} & \dfrac{\psi_{zz}}{\sqrt{2y}} \\ -f'\psi_y + \dfrac{f}{2y} & \dfrac{\psi_z}{2y} & -\dfrac{f'\psi_z}{\sqrt{2y}} \\ -\sqrt{2y}\psi_{yy} & 0 & -\psi_{yz} \end{pmatrix}\begin{pmatrix} a^y \\ a^\theta \\ a^z \end{pmatrix} + \begin{pmatrix} 0 & \dfrac{f}{2y} & 0 \\ -\dfrac{f}{2y} & 0 & 0 \\ 0 & 0 & 0 \end{pmatrix}\begin{pmatrix} a^y \\ a^\theta \\ a^z \end{pmatrix}, \quad (48)$$

where $\mathscr{I}$ is the identity matrix and $\mathscr{P}_{\mathbf{k}}$ is the projector on $\mathbf{k}$. The incompressibility condition (45) assumes a simple form

$$a^y k^y + a^\theta k^\theta + a^z k^z = 0. \quad (49)$$

Without loss of generality we can choose $\mathbf{x}_0$ in the form $\mathbf{x}_0 = (y_0, 0, 0)$.

Since the system of characteristic equations has a triangular structure, we solve them in succession. We start with Eq. (46) describing helical trajectories of the fluid particles. Projections of these trajectories onto the y, z-plane are closed. The period of rotation in the y, z-plane has the form

$$T(\psi) = \oint \frac{ds}{\sqrt{\psi_y^2 + \psi_z^2/2y}}. \quad (50)$$

Whether or not the trajectories themselves are closed depends on the ratio

$$Q(\psi) = \frac{1}{2\pi}\oint \frac{f\,ds}{2y\sqrt{\psi_y^2 + \psi_z^2/2y}}. \quad (51)$$

When this ratio is rational, the corresponding trajectories are closed; otherwise they cover the stream surface ergodically.

Next we consider Eq. (47) for the wave vector. This equation has a special structure which enables one to find a fundamental system of solutions explicitly. The analysis was carried out by Lifschitz and Hameiri [24]. They showed that this equation has a fundamental system of solutions $\mathbf{K}_i$, $i = 1, 2, 3$, two of which (say $\mathbf{K}_1$ and $\mathbf{K}_2$) are periodic with period T, and the third one, $\mathbf{K}_3$ grows linearly in time and becomes asymptotically proportional to $t\nabla\psi$. Accordingly, Eq. (47) has a two-parameter family of periodic solutions, while all other solutions grow linearly in time.

Consider now the transport equation (48) for the amplitude. We let $\mathscr{T}$ be the fundamental matrix solution of this equation, i.e., a solution satisfying the initial conditions $\mathscr{T}(0) = \mathscr{I}$. Since we have to restrict our consideration to the incompressible case we need to study the projections of $\mathscr{T}$ onto the subspace orthogonal to $\mathbf{k}$, i.e., to consider the projected fundamental matrix $\mathscr{T}_\pi = \mathscr{T}(\mathscr{I} - \mathscr{P}_{\mathbf{k}_0})$. The matrix $\mathscr{T}_\pi$ depends on $\mathbf{x}_0$ and $\mathbf{k}_0$.

The asymptotic behavior of this matrix at infinity ultimately determines the stability of the ring. It is shown in [24] that the norm of $\mathscr{T}_\pi$ can grow exponentially only when the initial data $\mathbf{k}_0$ is such that the corresponding wave vector $\mathbf{k}$ is periodic; otherwise is can only grow algebraically. Since the periodicity of the wave vector implies the periodicity of the coefficients of Eq. (48), it is natural to use Floquet theory in order to analyze the asymptotic behavior of $\mathscr{T}_\pi$ for a particular choice of $\mathbf{x}_0$, $\mathbf{k}_0$. One can construct the corresponding monodromy matrix, determine its eigenvalue v of largest absolute value, and define the local asymptotic growth rate as

$$\sigma_{\infty,\mathrm{loc}}(\mathbf{x}_0, \mathbf{k}_0) = \frac{1}{T}\log|v|. \quad (52)$$

It depends on $\mathbf{x}_0$, $\mathbf{k}_0$. However, it is independent of the magnitude of $\mathbf{k}_0$, as can be seen from (48), and we need to consider only unit vectors. In order to obtain the largest growth rate σ_∞ associated with the point $\mathbf{x}_0$, we have to consider all possible unit initial wave vectors $\mathbf{k}_0$ and maximize the value of $\sigma_{\infty,\mathrm{loc}}$ over them. The maximized growth rate σ_∞ so obtained depends only on the initial point $\mathbf{x}_0$. In fact, as a consequence of the asymptotic character of our definition of σ_∞, it depends only on the stream surface to which the initial point $\mathbf{x}_0$ belongs, so that $\sigma_\infty = \sigma_\infty(\psi)$.

For the purpose of comparing analytical and numerical results, the asymptotic behavior of the fundamental matrix solution $\mathscr{T}_\pi$ at infinity is less important than its finite-time behavior on a certain given time interval $0 \le t \le t^*$. We shall define a growth rate $\sigma_{t^*}(\psi)$ for this time interval to use rather than $\sigma_\infty(\psi)$. As a first step, we define, for each $\mathbf{x}_0$ and $\mathbf{k}_0$, the local finite-time growth rate by the formula

$$\sigma_{t^*,\mathrm{loc}}(\mathbf{x}_0, \mathbf{k}_0) = \frac{1}{2t^*}\log\|\mathscr{T}_\pi^{\mathrm{tr}}(t^*)\mathscr{T}_\pi(t^*)\|, \quad (53)$$

where $\mathscr{T}_\pi^{\mathrm{tr}}$ is the transpose of $\mathscr{T}_\pi$. The value of $\sigma_{t^*,\mathrm{loc}}(\mathbf{x}_0, \mathbf{k}_0)$, maximized over all unit initial vectors $\mathbf{k}_0$, gives the largest finite time growth rate $\bar{\sigma}_{t^*,\mathrm{loc}}(\mathbf{x}_0)$ associated with the point

$\mathbf{x}_0$. In contrast to the previous case, we can no longer say that this growth rate is the same for all points on a given stream surface. In order to obtain the growth rate σ_{t^*} which characterizes stream surfaces, we average $\tilde{\sigma}_{t^*,\mathrm{loc}}(\mathbf{x}_0)$ over various initial points $\mathbf{x}_0$ belonging to the same stream surface (with equal weights). It is this increment $\sigma_{t^*}(\psi)$ that we compare with the one observed in the numerical experiments described in Section 5.

Having these theoretical preliminaries in mind, we describe our numerical algorithm for studying the increments σ_{t^*}. First, we use the method described in the previous section to generate a vortex ring characterized by a certain choice of parameters (α, β, ζ). As a result, we obtain the values of ψ on the grid points inside the computational rectangle R. Then we extrapolate the values of ψ onto the intermediate points using the bicubic splines. In this way we obtain analytical expressions for ψ and its partial derivatives everywhere in R. Using these expressions we solve numerically Eq. (46) and determine the trajectory passing through the point $\mathbf{x}_0$. Next, we solve Eq. (47) and find three linearly independent solutions $\mathbf{K}_i$, $i = 1, 2, 3$, of the eikonal equation. To study the finite-time behavior of the solutions for one $\mathbf{x}_0$, we consider a two-parameter family of unit $\mathbf{k}_0$ of the form

$$\mathbf{k}_0 = \cos\mu \sin\nu\mathbf{K}_1(0) + \sin\mu \sin\nu\mathbf{K}_2(0) + \cos\nu\mathbf{K}_3(0) \quad (54)$$

and compute the corresponding projected fundamental solution for Eq. (48). We find $\sigma_{t^*,\mathrm{loc}}(\mathbf{x}_0, \mathbf{k}_0)$ for various μ, ν using formula (53). We scan the μ, ν-parameter space and find the maximum finite-term growth rate $\tilde{\sigma}_{t^*,\mathrm{loc}}(\mathbf{x}_0)$. Finally we average this for $\mathbf{x}_0$ along the stream surface to obtain $\sigma_{t^*}(\psi)$. The resulting values are reported for several rings in Section 5. We emphasize that for a fixed time t^* the short-term growth rate can be considerably larger than the asymptotic growth rate σ_∞.

Once the growth rates of these instabilities have been calculated, we can compare them with the results of time-dependent numerical simulations. This gives us an opportunity to determine the general applicability of the approximations made in this section. In the next section we discuss the type and size of the initial perturbations which we impose.

4. VORTEX METHODS

The numerical solutions of the time-dependent Euler equations in this paper are computed using a three-dimensional vortex method. Methods of this type have been used for some time [8, 9, 19, 20]; see [17, 31] for recent surveys. Essentially the version used here and described in this section was introduced by Anderson and Greengard [1]. It was shown to converge to the exact solution by Beale [4] and Cottet [10]; see [6] for earlier theory and Hald's article in [17] for a fuller treatment. Like all three-dimensional vortex methods, this version is based on the Biot–Savart law, which expresses velocity $\mathbf{u}$ in terms of the vorticity $\boldsymbol{\omega}$. This results in evolution equations for the position $\mathbf{x}$ and the vorticity $\boldsymbol{\omega}$, reducing the Euler equations to a system of nonlinear ordinary differential equations. Several numerical studies of three-dimensional flow have been carried out using vortex methods; further references include [5, 18, 26, 27, 41]. While these have contributed to the understanding of inviscid fluid dynamics, including some comparison with analytical predictions or experimental data, more experience is needed with the performance of these methods in general. The availability of exact solutions such as the vortex rings with swirl affords such an opportunity. In this section, we describe the numerical method, and then present several simulations of vortex rings. We also describe two modifications designed to help reduce numerical errors. One modification is a regridding procedure which can improve accuracy at later times, as demonstrated here, but it will not be used for measuring the growth of perturbations. The second modification eliminates the steady solution in order to calculate perturbations specifically. It is used in the next section to compare with the growth rate predictions in Section 3. At the end of the present section, we describe this approach and also the form of the perturbation to be introduced.

The vortex method we develop here is a general one for solutions of the Euler equations and does not depend specifically on the structure of the rings. Fourfold symmetry is exploited to reduce the computational load by a factor of 4; when initial conditions with fourfold symmetry are imposed the results are identical to those which do not exploit symmetry. To lower the computational load further, we use a fast summation algorithm [7, 15, 16] to reduce the operation count of the method; see below. To motivate the Biot–Savart law we observe that, if the velocity $\mathbf{u}$ is zero at infinity, the divergence condition suggests the existence of a vector stream function $\boldsymbol{\Psi}$ so that

$$\nabla \times \boldsymbol{\Psi} = \mathbf{u}. \quad (55)$$

If we assume that $\boldsymbol{\Psi}$ is divergence-free and take the curl, we obtain

$$-\nabla^2\boldsymbol{\Psi} = \boldsymbol{\omega}. \quad (56)$$

To solve this equation, we write $\boldsymbol{\Psi}$ in terms of the Green's function of the Poisson equation in three dimensions,

$$\boldsymbol{\Psi}(\mathbf{x}, t) = \int G(\mathbf{x} - \mathbf{x}')\boldsymbol{\omega}(\mathbf{x}', t)\, d\mathbf{x}', \quad (57)$$

where $\mathbf{x}'$ is the location of the volume element $d\mathbf{x}'$ and

$$G(\mathbf{x}) = \frac{1}{4\pi r}, \quad r = |\mathbf{x}| \tag{58}$$

Finally, we take the curl of this equation to obtain the well-known Biot–Savart law,

$$\mathbf{u}(\mathbf{x}, t) = \int K(\mathbf{x} - \mathbf{x}', t)\boldsymbol{\omega}(\mathbf{x}', t)\, d\mathbf{x}' \tag{59}$$

$$K(\mathbf{x}) = -\frac{\mathbf{x}}{4\pi r^3} \times .$$

This provides an evolution equation for the position of particles in the flow, when the vorticity is known. The second evolution equation is the vorticity transport equation, the curl of the first Euler equation (1), which can be written in the form

$$\frac{D\boldsymbol{\omega}}{Dt} = \boldsymbol{\omega} \cdot \nabla \mathbf{u}, \tag{60}$$

where $D\boldsymbol{\omega}/Dt = \partial\boldsymbol{\omega}/\partial t + \mathbf{u} \cdot \nabla\boldsymbol{\omega}$ is the material derivative.

We now use these evolution equations to produce a numerical method. The integral in the Biot–Savart law is over all space, but for the case of the vortex ring the integral is only performed over the vortex core, the bounded set where the vorticity $\boldsymbol{\omega}$ is nonzero. To integrate numerically we introduce a square grid of size h covering the vortex core. Grid points correspond to initial locations of representative particles, with a known initial vorticity. In a Lagrangian scheme, we then follow these elements as they move along particle paths. Particle positions and vorticities will be labeled as $\mathbf{x}_j(t)$ and $\boldsymbol{\omega}_j(t)$, respectively. We approximate the velocity field produced by the Biot–Savart law as

$$\mathbf{u}^h(\mathbf{x}, t) = \sum_j K_\delta(\mathbf{x} - \mathbf{x}_j)\boldsymbol{\omega}_j h^3, \tag{61}$$

where K_δ is a smooth version of the kernel of (59), described below. We use this velocity field to provide an evolution equation for the position $\mathbf{x}_i$ of each particle

$$\frac{d\mathbf{x}_i}{dt} = \mathbf{u}^h(\mathbf{x}_i, t) = \sum_j K_\delta(\mathbf{x}_i - \mathbf{x}_j)\boldsymbol{\omega}_j h^3. \tag{62}$$

Since the particle $\mathbf{x}_i$ is moving with the flow, its vorticity evolution can be approximated by

$$\frac{d\boldsymbol{\omega}_i}{dt} = \boldsymbol{\omega}_i \cdot \nabla \mathbf{u}_i^h \tag{63}$$

using (60). The derivative $\nabla \mathbf{u}_i^h$ can be obtained by observing that the dot product reduces to a directional derivative; we replace this derivative with a centered difference quotient. While there are other possible evolution equations for the vorticity, the one presented here is the most conceptually simple, is the simplest to implement, and seems to produce the best numerical results (see [5] for a discussion).

One of the difficulties in using the method described above arises in the quadrature of the singular integral for the velocity field. Notice that the velocity is determined by what is essentially an inverse square law which implies the effects of the discretization will be pronounced near a particle location. To deal with this problem it is common to introduce vortex blobs, replacing point vortices with smooth overlapping regions of vorticity. A smooth version of the kernel K in (59) is introduced as $K_\delta = K * \phi_\delta$, where $\phi_\delta = \delta^{-3}\phi(x/\delta)$, ϕ is a shape function of total weight one and δ is the vortex blob size. This size should be large enough to allow nearby vortex blobs to overlap but small enough to avoid smearing the results. Since Eq. (62) produces good results for distant points without modification, it will also be desirable to choose a shape function which does not modify K for large values of r. There are several criteria for choosing a shape function ϕ which is as nondisruptive as possible but still provides the smoothing required. These criteria are described in more detail in [6]; however, a short discussion is presented here.

Since $K_\delta = \mathrm{K} * \phi_\delta$ and $K = \nabla \times G$, where G is the Green's function for $-\nabla^2$, we know that $K_\delta = \nabla \times G_\delta$, where $G_\delta = G * \phi_\delta$. This along with Eq. (58) implies

$$K_\delta(\mathbf{x}) = \frac{\partial G_\delta(r)}{\partial r}\frac{\mathbf{x}}{r} \times, \tag{64}$$

where $r = |\mathbf{x}|$. The fact that G is the Green's function for $-\nabla^2$ also implies that

$$-\nabla^2 G_\delta = \phi_\delta. \tag{65}$$

To determine $\phi = \phi_1$ we simplify the problem by assuming that

$$K_1(\mathbf{x}) = -\frac{f(r)\mathbf{x}}{4\pi r^2} \times, \tag{66}$$

where f is to be determined. If this is true then

$$\frac{\partial G_1(r)}{\partial r} = -\frac{f(r)}{4\pi r^2}. \tag{67}$$

We use this to show that

$$\phi = \phi_1 = -\nabla^2 G_1 = -\frac{1}{r^2}\frac{\partial}{\partial r}\left(r^2 \frac{\partial G_1}{\partial r}\right) = \frac{f'(r)}{4\pi r^2}. \tag{68}$$

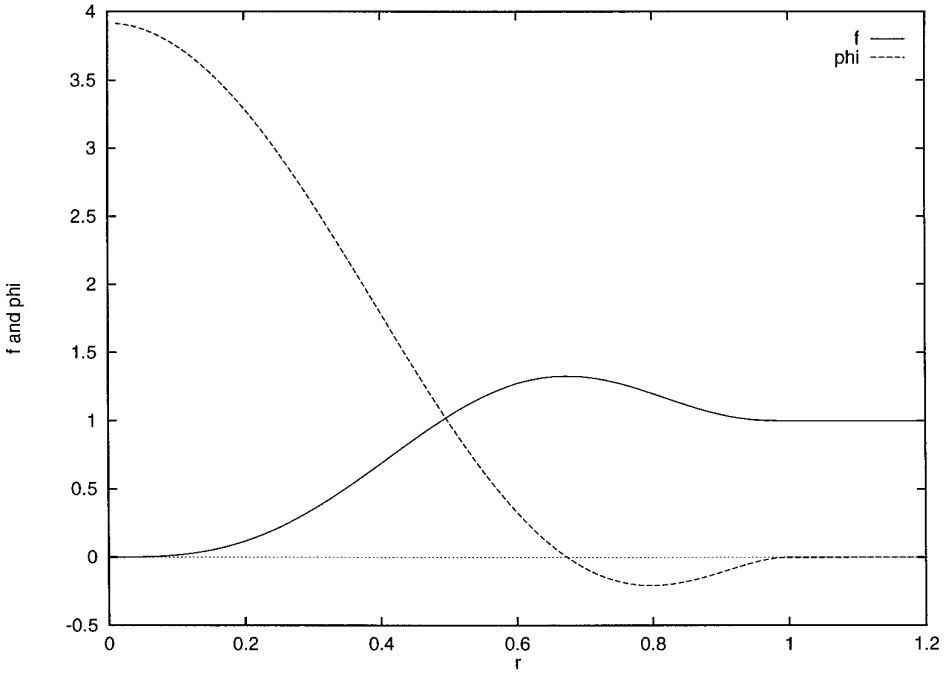

FIG. 4. The shape function: ϕ and f.

The conditions we impose on ϕ and f ensure that ϕ is smooth, has weight one, and is fourth-order accurate (see [4–6] for a discussion of order). We also require that ϕ have compact support so we can use the fast summation algorithm described later. Thus, we require that $f'(r)$ be a continuous function of r^2, $f(r) = O(r^3)$ as $r \to 0$, $f(r) = 1$ for $r \geq 1$, and $\int \phi(r)\, r^4\, dr = 0$. Assuming that ϕ is a third-degree polynomial in r^2 for $r \leq 1$ and zero for $r \geq 1$, we see that $f(r) = O(r^3)$ as $r \to 0$. We now have four coefficients to choose and only three additional requirements to meet. This allows one degree of freedom with which to choose a function with a small amplitude and derivative. One such function is

$$\phi = \frac{1}{4\pi}\begin{cases} \frac{1}{32}(-3465r^6 + 8505r^4 - 6615r^2 + 1575), & r \leq 1 \\ 0, & r \geq 1. \end{cases} \tag{69}$$

This is the shape function which will be used for the duration of this paper. This ϕ and its corresponding f are plotted in Fig. 4. The moment condition for fourth-order accuracy requires a change of sign in ϕ. Further cancellation would be undesirable, and this choice of ϕ has a reasonable combination of the needed properties.

Once the vortex blobs with the shape function are introduced, the evolution of the flow reduces to a specific system of ordinary differential equations

$$\begin{aligned} \frac{d\mathbf{x}_i}{dt} &= \mathbf{u}^h(x_i, t) = \sum_j K_\delta(\mathbf{x}_i - \mathbf{x}_j)\mathbf{w}_j h^3 \\ \frac{d\boldsymbol{\omega}_i}{dt} &= \boldsymbol{\omega}_i \cdot \nabla \mathbf{u}_i^h \end{aligned} \tag{70}$$

where $K_\delta = K * \phi_\delta$, $\phi_\delta = \delta^{-3}\, \phi(x/\delta)$, and ϕ is given by Eq. (69). This system can be discretized in time by a variety of ordinary differential equation solvers. Here the classical fourth-order Runge–Kutta method was chosen since its stability region includes a large portion of the imaginary axis, and because it has been found to work well in practice with fairly large time steps.

Without further modification, this vortex method is computationally quite expensive. In Eq. (70) we see that the vorticity of every particle effects the velocity of every other particle, resulting in order n^2 terms, where n is the number of representative particles. Since the problem is fully three-dimensional the number of grid points can become quite large, even at modest grid sizes. It is desirable to reduce the operation count of the method using a fast summation algorithm. Because of the inverse square character of particle interactions it is reasonable to use a multipole expansion to approximate the influences of a group of distant particles. Methods of this type can reduce the order of vortex methods from n^2 to n. Such an algorithm has been developed by Greengard and Rokhlin [16, 15]. However, the complexity of this algorithm seems to make it most useful for a very large number of particles. In this paper

we use a simplification developed and programmed by Buttke; see [7] for a discussion. This method reduces the computational count from order n^2 to order $n^{3/2}$ and is practical for a moderate number of particles. The algorithm breaks the region under consideration into a number of large boxes. To find the sum of all influences on a given particle, the influences from particles in nearby boxes are calculated individually, and the effects of particles in boxes farther away are represented by multipole expansions. The velocities calculated using this method can be made to agree with arbitrary accuracy to those calculated using direct summation.

We now present the results of time-dependent calculations, using the method just described, for three unperturbed vortex rings. These results illustrate the behavior of the rings and the performance of the method. For comparison, some calculations have been done using a regridding procedure, described below. Fourfold symmetry and fast summation are used in all cases. The solution is initialized with a numerically exact ring, found from the method described in Section 2. No intentional perturbation is introduced. To evaluate these results, the velocity $\mathbf{u}_s(\mathbf{x}_i)$ of the steady vortex ring is calculated, using the computed stream function ψ and Eq. (6), at 100 points $\mathbf{x}_i$ chosen on each of three rectangular cross sections of the vortex core. At every time step, the time-dependent velocity $\mathbf{u}(\mathbf{x}_i)$ is calculated at these points using the first equation of (70). These velocities are then compared to find a relative L^2 velocity error

$$E_u = \left(\frac{\sum_i |\mathbf{u}(\mathbf{x}_i) - \mathbf{u}_s(\mathbf{x}_i)|^2}{\sum_i |\mathbf{u}_s(\mathbf{x}_i)|^2} \right)^{1/2}. \tag{71}$$

Our first example is a ring which was used in a similar calculation by Beale, Eydeland, and Turkington [5]. This ring was under resolved in the earlier work. Here it is better resolved because of the improvements described in Section 2, and we show that it is particularly unstable. Our other two examples are much more stable. The first vortex ring, Ring 1 in Fig. 5, is produced using the method of Section 2 with $\alpha = 512$, $\beta = 0$, and $\zeta = 3$. It is a Beltrami ring propagating along the z-axis with velocity 0.144. Its cross section is roughly circular with $0.86 < r < 1.88$ and $|z| < 0.57$. Here we return to the usual cylindrical coordinates (r, θ, z). The grid size is $h = 0.075$, the vortex blob size is $\delta = 0.32$, and the time step is $\Delta t = 0.2$. Approximately 5000 particles are used in $\frac{1}{4}$ of the ring. When regridding was allowed, the error jumped each time the regridding occurred, but the overall growth rate of the velocity error was reduced. This seems to indicate that the regridding improved the long time behavior of the numerical simulation.

The second ring, ring 2 in Fig. 6, is produced with $\alpha = 20$, $\beta = 10$, and $\zeta = 1.5$. It is intermediate with respect to swirl and is much more stable. As noted in Section 2, much of this stability originates in the smaller value of ζ. While larger values of ζ increase the smoothness of the stream function ψ at the boundary of the vortex core, they also increase its complexity and produce less stable rings. The ring is propagating along the z-axis with velocity 0.121 and has a roughly circular cross section with $0.67 < \mathrm{r} < 2.03$ and $|z| < 0.82$. The grid size is $h = 0.1$, the vortex blob size is $\delta = 0.37$, and the time step is $\Delta t = 0.2$. Again, about 5000 particles are used. The results, shown in Fig. 6, demonstrate the stability which can be obtained for vortex rings with swirl.

The third ring is produced with $\alpha = 50$, $\beta = 0$, and $\zeta = 1.5$ and is included here to illustrate the degree of stability obtainable with Beltrami rings. It propagates along the z-axis with velocity 0.119 and has a cross section with $0.88 < r < 1.93$ and $|z| < 0.60$. There is no intentional initial perturbation. The vortex blob size is $\delta = 0.32$ and the grid size is $h = 0.075$ resulting in $n = 8229$ initial representative particles in $\frac{1}{4}$ of the vortex ring. The calculation of the third ring used regridding. The results, along with those for ring 2, are shown in Fig. 6.

One source of errors, due to the Lagrangian nature of the method, is that the sum (61) used in the approximation to the Biot–Savart law (59) depends on the varying particle locations. This problem is partially solved using vortex blobs. A regridding procedure can be used to further ensure an even distribution of vorticity. At times chosen by some criterion, the vorticity is redistributed to new particles which start on a square grid. The new vorticities can be calculated from the old values using the formula

$$\boldsymbol{\omega}^*(\mathbf{x}) \approx \sum_j \boldsymbol{\omega}_j \phi_\delta(|\mathbf{x} - \mathbf{x}_j|). \tag{72}$$

In the calculations just discussed, the decision to regrid was based on a calculation of the vorticity at the particle locations, found from (72). These values were compared with the $\boldsymbol{\omega}_i$. Regridding was carried out if the relative L^2 error exceeded 180%. For the first ring, this occurred five times, since the ring was quite unstable, while for the second it only occurred twice. While regridding has advantages which are evident in these results, it smears the answer, if done often, and increases the computational region. Thus the number of particles, and the computational effort, increase in time. For the instability calculations in the next section, we do not use regridding but another modification instead.

Since we are interested in the evolution of perturbations, we introduce a modification in the numerical method which allows us to eliminate the steady part of the problem. We impose an initial velocity perturbation $\mathbf{u}_0(\mathbf{x})$ and its

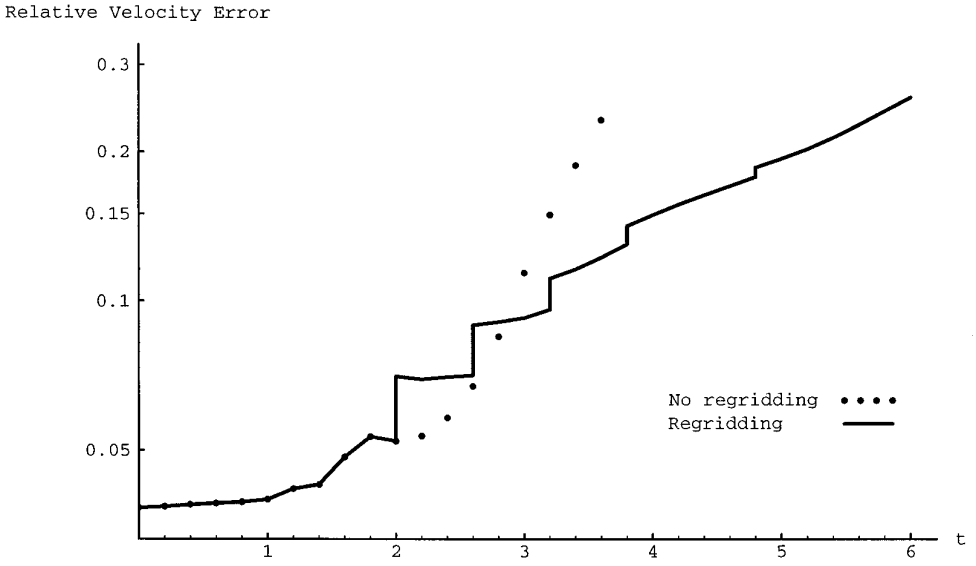

FIG. 5. Relative velocity error for ring 1.

associated vorticity perturbation $\boldsymbol{\omega}_0(\mathbf{x})$ on the velocity and vorticity fields, $\mathbf{u}_s(\mathbf{x})$ and $\boldsymbol{\omega}_s(\mathbf{x})$, of a steady vortex ring. We want to find $\mathbf{u}(\mathbf{x}, t)$ so that $\mathbf{u}(\mathbf{x}, 0) = \mathbf{u}_0(\mathbf{x})$ and $\mathbf{u}_s(\mathbf{x}) + \mathbf{u}(\mathbf{x}, t)$ is a solution to the Euler equations (1). The corresponding vorticity perturbation is $\boldsymbol{\omega}(\mathbf{x}, t) = \nabla \times \mathbf{u}$. Since this process does not depend on any vortex ring structure, it could be used to model the behavior of perturbations of any steady solution of the Euler equations.

If $\mathbf{u}_s + \mathbf{u}$ satisfies the Euler equations and $\boldsymbol{\omega}_s + \boldsymbol{\omega} = \nabla \times (\mathbf{u}_s + \mathbf{u})$, then $\boldsymbol{\omega}_s + \boldsymbol{\omega}$ and $\mathbf{u}_s + \mathbf{u}$ must satisfy (60) and (59), leading to

$$\frac{\partial(\boldsymbol{\omega}_s + \boldsymbol{\omega})}{\partial t} + (\mathbf{u}_s + \mathbf{u}) \cdot [\nabla(\boldsymbol{\omega}_s + \boldsymbol{\omega}) = (\boldsymbol{\omega}_s + \boldsymbol{\omega}) \cdot \nabla(\mathbf{u}_s + \mathbf{u}),$$
$$(\mathbf{u}_s + \mathbf{u}) = \int K(\mathbf{x} - \mathbf{x}')(\boldsymbol{\omega}_s(\mathbf{x}', t) + \boldsymbol{\omega}(\mathbf{x}', t))\, d\mathbf{x}'. \tag{73}$$

Since $\mathbf{u}_s$ also satisfies the Euler equations, this simplifies to

$$\frac{D\boldsymbol{\omega}}{Dt} = (\boldsymbol{\omega}_s + \boldsymbol{\omega}) \cdot \nabla \mathbf{u} + \boldsymbol{\omega} \cdot \nabla \mathbf{u}_s - \mathbf{u} \cdot \nabla \boldsymbol{\omega}_s,$$
$$\mathbf{u}(x, t) = \int K(\mathbf{x} - \mathbf{x}')\, \boldsymbol{\omega}(\mathbf{x}', t)\, d\mathbf{x}', \tag{74}$$

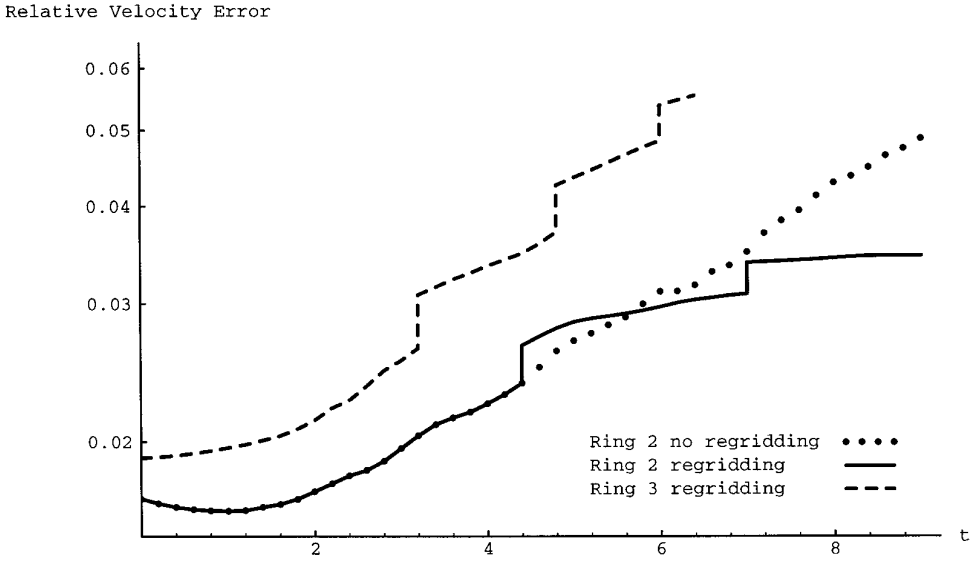

FIG. 6. Relative velocity error for rings 2 and 3.

where $D\boldsymbol{\omega}/Dt = (\mathbf{u}_s + \mathbf{u}) \cdot \nabla\boldsymbol{\omega}$ is the material derivative. We then discretize the problem to a system of evolution equations similar to the unmodified method,

$$\begin{aligned}\frac{d\mathbf{x}_i}{dt} &= \mathbf{u}_s(\mathbf{x}_i) + \sum_j K_\delta(\mathbf{x}_i - \mathbf{x}_j)\boldsymbol{\omega}_j h^3,\\ \frac{d\boldsymbol{\omega}_i}{dt} &= (\boldsymbol{\omega}_s(\mathbf{x}_i) + \boldsymbol{\omega}_i)\cdot\nabla\mathbf{u}^h(\mathbf{x}_i, t)\\ &\quad + \boldsymbol{\omega}_i\cdot\nabla\mathbf{u}_s(\mathbf{x}_i) - \mathbf{u}^h(\mathbf{x}_i, t)\cdot\nabla\boldsymbol{\omega}_s(\mathbf{x}_i),\end{aligned} \tag{75}$$

which we solve using the fourth-order Runge–Kutta method. We obtain the steady velocity $\mathbf{u}_s$ and vorticity $\boldsymbol{\omega}_s$ to any accuracy desired using Eq. (6) and a differencing scheme to approximate derivatives of the stream function ψ. The gradients in (75) can be interpreted as directional derivatives and are also approximated using difference quotients.

We must now introduce an initial perturbation $\mathbf{u}(\mathbf{x}, 0) = \mathbf{u}_0(\mathbf{x})$ in velocity and $\boldsymbol{\omega}(\mathbf{x}, 0) = \boldsymbol{\omega}_0(\mathbf{x}) = \nabla \times \mathbf{u}_0(\mathbf{x})$ in vorticity. In principle we can vary the wavelength, shape, direction, and location of our initial perturbations. We will not attempt a comprehensive study, but instead we focus on the behavior of specific small amplitude perturbations which can be compared with the instability predictions of Section 3. The perturbation we describe now is used in Section 5 to initialize the calculations of time-dependent solutions for various perturbed rings.

The vortex core is the region where the stream function ψ is greater than zero, and ψ roughly measures the depth inside the core. Thus it is reasonable to use a cutoff function of ψ to limit our initial perturbation to the immediate neighborhood of the vortex core. Here we use the cutoff function

$$\Gamma(\psi) = \begin{cases} 10\exp(-8), & \psi > \psi_c \\ 10\exp\left(\dfrac{-0.0008}{0.01^2 - (\psi_c - \psi)^2}\right), & \psi_c \geq \psi > (\psi_c - 0.01) \\ 0, & \psi \leq (\psi_c - 0.01), \end{cases} \tag{76}$$

where the cutoff value, ψ_c, is one tenth of the maximum value of ψ. This function confines the initial perturbation to the region, where $\psi > (\psi_c - 0.01)$. A typical ring in this study has a stream function which varies, inside the vortex core, from 0 to approximately 0.1. The perturbation has an amplitude of $10\exp(-8) \approx 0.00335$, approximately 1% of the maximum velocity for the rings in this paper.

The solution of the system (75) is initialized by a vorticity perturbation $\boldsymbol{\omega}_0$, determined as the curl of an initial velocity perturbation, $\mathbf{u}_0$, which we specify. We introduce a wave function in θ with wave number 20, a multiple of four which allows us to exploit fourfold symmetry. If we choose the $\hat{r}$ direction, the resulting velocity perturbation has the form

$$\mathbf{u}_0 = \Gamma(\psi)\cos(20\,\theta)\hat{r}. \tag{77}$$

Taking the curl, we arrive at the initial vorticity perturbation

$$\begin{aligned}\boldsymbol{\omega}_0 &= \frac{\partial}{\partial z}(\Gamma(\psi)\cos(20\,\theta))\hat{\theta} - \frac{1}{r}\frac{\partial}{\partial\theta}(\Gamma(\psi)\cos(20\,\theta))\hat{z}\\ &= \frac{d\Gamma(\psi)}{d\psi}\frac{\partial\psi}{\partial z}\cos(20\,\theta)\hat{\theta} + \frac{20}{r}\Gamma(\psi)\sin(20\,\theta)\hat{z},\end{aligned} \tag{78}$$

where all of the derivatives in this equation are approximated as difference quotients in ψ.

5. TIME-DEPENDENT VORTEX RING SIMULATIONS

In this section we compare the results of computations using the modified vortex method of Section 4 with the the instability predictions of Section 3. We study the evolution of perturbations to a two-parameter family of vortex rings, which are calculated using the procedure described in Section 2. Maximum growth rates for these specific rings, depending on the location in the ring, are found using the WKB analysis explained in Section 3. Time-dependent perturbations to the Euler equations are then computed for these rings by the modified vortex method, using the initial perturbation given in Section 4. The rates of growth for these perturbations are compared with the analytical predictions, and the results are interpreted. Generally, the computed rates are somewhat lower than the predicted

TABLE I

Observed and Predicted Growth Rates with $\alpha = 50$ and $\beta = 20$

Level number i	Value of ψ_i	Period T	Growth rate	
			Predicted	Observed
1	0.0103	21.6	0.338	0.148
2	0.0207	18.2	0.370	0.153
3	0.0310	15.6	0.387	0.155
4	0.0414	13.7	0.396	0.151
5	0.0517	12.2	0.396	0.151
6	0.0620	10.9	0.384	0.151
7	0.0724	9.94	0.351	0.147
8	0.0827	9.09	0.292	0.137
9	0.0931	8.37	0.199	0.119
10	0.1034	7.76	0.111	0.076

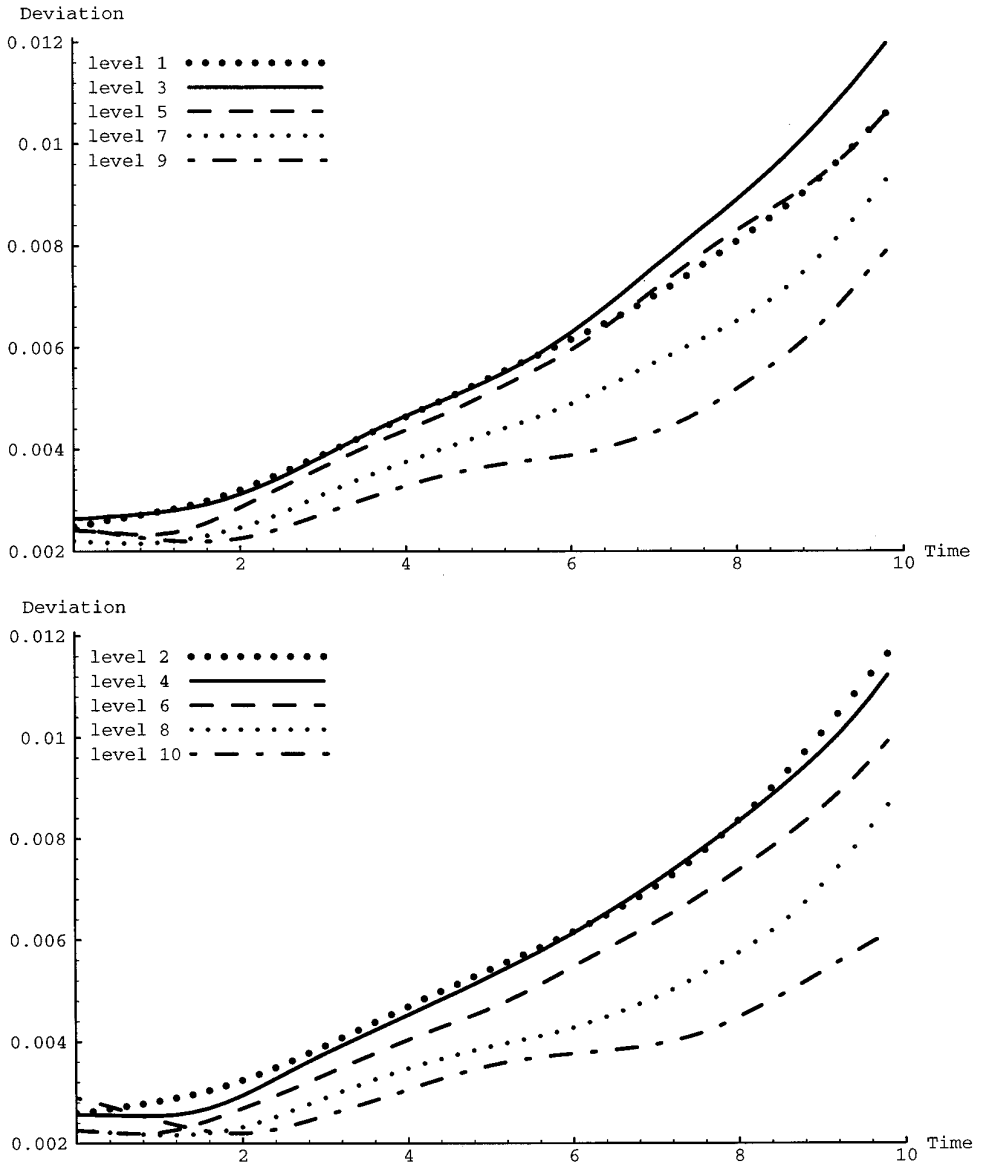

FIG. 7. Perturbation growth of the ring with $\alpha = 50$ and $\beta = 20$.

maximum, and the dependence on location and ring parameters is consistent with the predictions.

In order to compare the two kinds of results, we need to compute localized growth rates in the vortex method simulation which are compatible with those predicted by the analysis for different regions of the vortex ring. We examine the perturbation evolution near a level curve of the stream function ψ by identifying representative particles located near the curve and following their evolution in time. Since neither the initial grid points or the particle locations in the vortex method are convenient for this purpose, we introduce special tracking particles which are located near the level curve. While these tracking particles are carried along with the flow and their velocities and positions are computed, they are not used in the vortex method calculation.

We need a convenient coordinate system in which to identify these tracking particles. In a vortex ring the level sets of ψ form a family of nested tori, with the inner most being the circle on which $\psi = \psi_{\max}$, the maximum value of ψ. This circle is given in cylindrical coordinates by $r = r_0$, $z = z_0$, and $0 \le \theta < 2\pi$. In our new coordinate system, we leave the θ unchanged and replace r and z with ψ and ϕ, where $0 < \psi \le \psi_{\max}$, and $0 \le \phi < 2\pi$ identifies the angle in the poloidal cross section of the ring, centered around the location of $\psi_{\max}$. This coordinate system

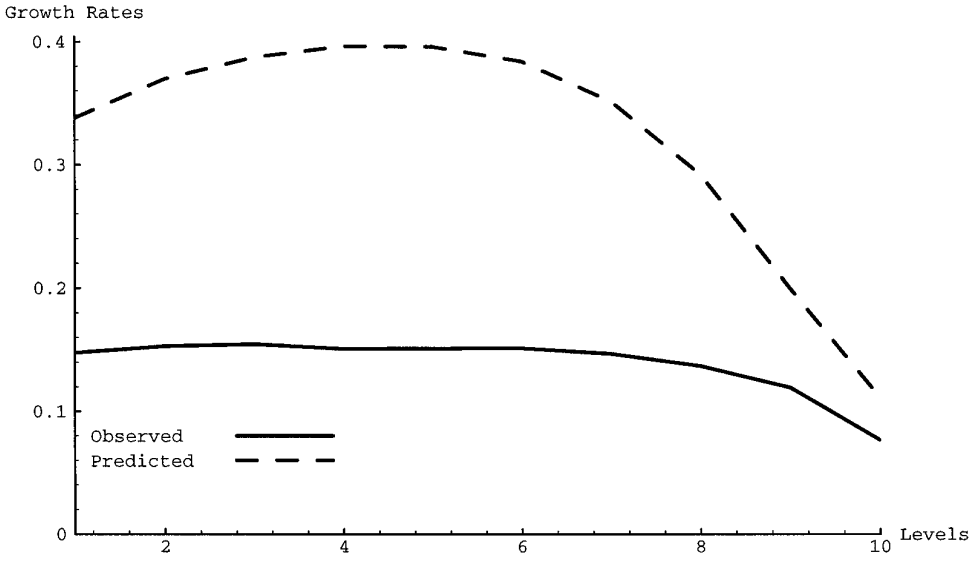

FIG. 8. Observed and predicted growth rates with $\alpha = 50$ and $\beta = 20$.

uniquely identifies the points of the vortex core as long as the stream function has only one maximum, as it does for the rings in this study. The tracking particles are initially placed along the level sets of ψ at the points $(\psi_i, \theta_j, \phi_k)$ given by

$$\psi_i = \frac{i\psi_{\max}}{10}, \quad \theta_j = \frac{(\pi/2)(10-j)}{10}, \quad \phi_k = \frac{2\pi(10-k)}{10}, \quad (79)$$

where $1 \le i, j, k \le 10$ are integers. Because of fourfold symmetry, we identify 1000 tracking particles in the quarter of the ring where $0 \le \theta < \pi/2$. In each poloidal cross section we move the 10 tracking particles located at $\psi = \psi_{\max}$ out slightly to $\psi = 0.99\ \psi_{\max}$. The particles are relabeled, with those for each level in ψ listed in some order, so that $\mathbf{x}_j^i$ is the jth particle associated with ψ_i. A relative velocity deviation

$$E_u^i = \left(\frac{\sum_j |\mathbf{u}_j^i|^2}{\sum_j |\mathbf{u}_s(\mathbf{x}_j^i) + \mathbf{u}_j^i|^2} \right)^{1/2} \quad (80)$$

can now be calculated for the particles associated with ψ_i, where $\mathbf{u}_j^i$ is the velocity perturbation and $\mathbf{u}_s(\mathbf{x}_j^i)$ is the exact steady velocity at the point $\mathbf{x}_j^i$.

We now introduce the two-parameter family of vortex rings for which we will calculate the deviation as just described. This family arises from the parameters α and β in the structure functions (17). We examine separately the rings in the one-parameter family where $\alpha = 20, 50, 80$ while $\beta = 20$ is fixed, and the family $\beta = 0, 20, 40$ while $\alpha = 50$. For all of these rings the parameter $\zeta = 1.5$. The perturbed solutions are calculated until $t = 9.8$. This is roughly the period of a particle near the center of the ring moving in the poloidal cross section. The time step is $\Delta t = 0.2$; a smaller time step was found to have very little effect. The vortex blob size in (70) is $1.17\sqrt{h}$, where h is the grid size. Fast summation and fourfold symmetry are used in all calculations. The initial perturbation is that discussed at the end of Section 4. An exponential rate of growth for the velocity deviation (80) in each stream surface is derived from its change during the elapsed time. These are presented in the figures and tables as "Observed" growth rates and compared with the "Predicted" growth rates from the WKB theory. As explained in Section 3, the predicted rate $\sigma_t * (\psi)$ is found by computing the local rate of (53), maximizing over $\mathbf{k}_0$, and then averaging over the stream surface.

The vortex ring common to both groups has the parameters $\alpha = 50$, $\beta = 20$. This ring has a stream function with maximum value $\psi_{\max} = 0.103$ and a propagation velocity 0.0671. The periods of rotation T (50) of representative particles on various stream surfaces are given in Table I. The grid size is $h = 0.08$ which results in 4270 grid points in a quarter of the ring. The perturbation growth (80) as

TABLE II

Information on a Family Varing in α

α	h	n	Prop. speed	$\psi_{\max}$	$T_{\min}$
20	0.10	3976	0.0637	0.101	14.0
50	0.08	4270	0.0671	0.103	7.76
80	0.08	2955	0.0702	0.104	5.35

TABLE III

Growth Rates for a Family Varying in α

	$\alpha = 20$		$\alpha = 50$		$\alpha = 80$	
Level	Predicted	Observed	Predicted	Observed	Predicted	Observed
1	0.180	0.0298	0.338	0.148	0.470	0.276
2	0.199	0.0287	0.370	0.153	0.522	0.280
3	0.211	0.0228	0.387	0.155	0.599	0.281
4	0.218	0.0274	0.396	0.151	0.572	0.284
5	0.219	0.0315	0.396	0.151	0.558	0.290
6	0.212	0.0344	0.384	0.151	0.530	0.297
7	0.196	0.0377	0.351	0.147	0.495	0.302
8	0.176	0.0380	0.292	0.137	0.445	0.298
9	0.141	0.0288	0.199	0.119	0.350	0.280
10	0.103	0.0158	0.111	0.076	0.169	0.249

a function of time is plotted in Fig. 7; notice that for clarity alternating levels are plotted on different graphs. The levels are indexed by i, where the stream function has the value ψ_i. Observed and predicted growth rates between $t = 0$ and $t = 9.8$ are listed in Table I and graphed in Fig. 8.

In interpreting the growth rates, it is important to remember that the WKB method predicts a maximum growth rate over all initial perturbations while the vortex method calculates the growth rate for one perturbation in particular. The WKB-type method also describes the growth of short wavelength local instabilities. Longer wavelength perturbations and nonlocal effects may play a large role in the evolution of a vortex ring. Nonlocal effects, which can be clearly seen in the Biot–Savart law (59), are particularly important as a stabilizing influence, for without them the ring would not be a steady structure in time. Notice, in Fig. 8, that the predicted growth rates vary more than the observed growth rates. It seems reasonable that nonlocal effects force perturbations in different locations to grow at similar rates. It is, in fact, surprising that the observed and predicted growth rates match as closely as they do here.

We now examine the one-parameter family where $\alpha = 20, 50, 80$, and $\beta = 20$. The calculations use different mesh sizes, but all have approximately 3000–4000 representative particles in $\frac{1}{4}$ of the vortex ring. Specific information about these rings is contained in Table II which lists mesh size h, the number of representative particles in $\frac{1}{4}$ of the ring n, the propagation speed, the maximum value of the stream function $\psi_{\max}$, and the minimum period of rotation $T_{\min}$.

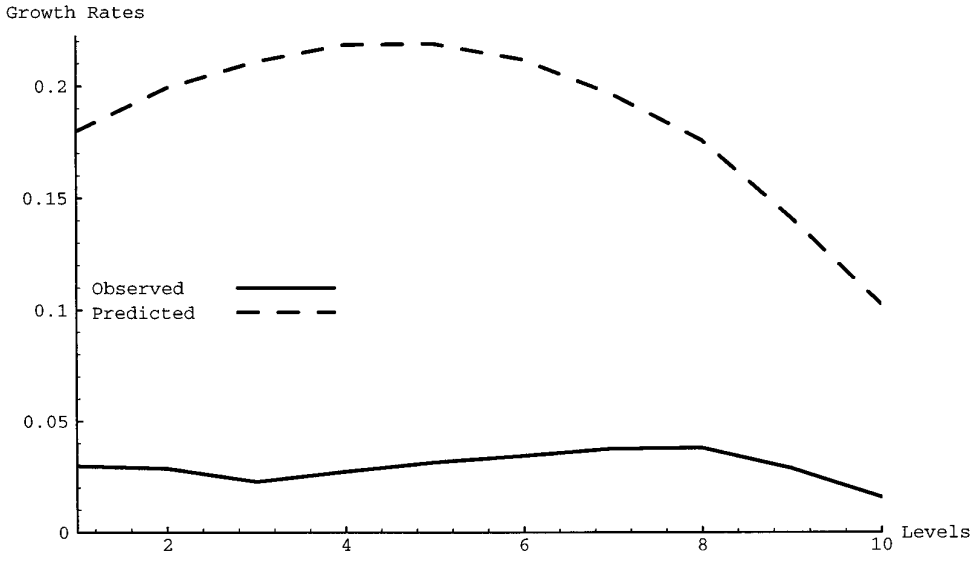

FIG. 9. Observed and predicted growth rates with $\alpha = 20$ and $\beta = 20$.

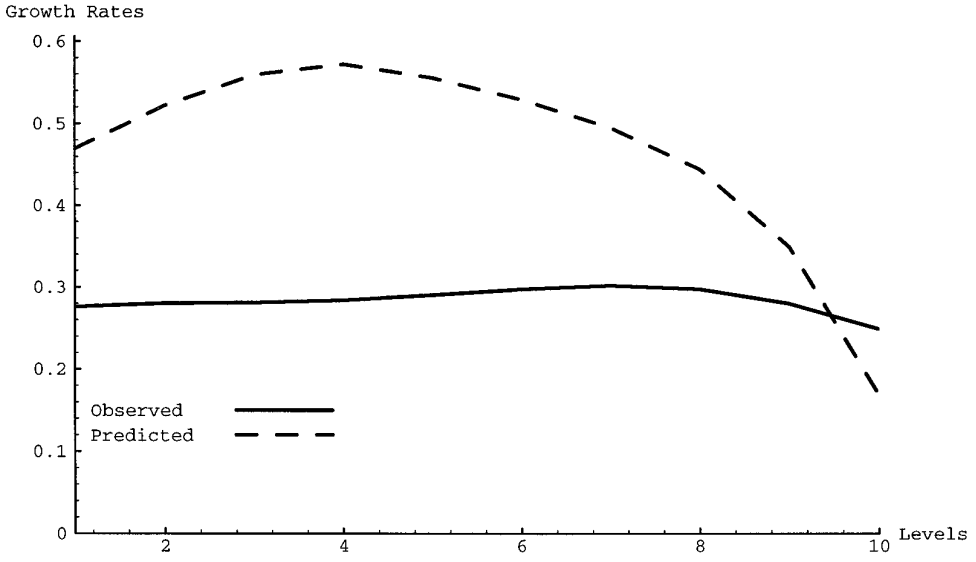

FIG. 10. Observed and predicted growth rates with $\alpha = 80$ and $\beta = 20$.

The average and predicted growth rates are given in Table III. We have already seen the results for the ring where $\alpha = 50$ and the results for the rings with $\alpha = 20$ and $\alpha = 80$ are plotted in Figs. 9 and 10.

Notice that the predicted maximum growth rate is generally two to three times larger than the observed growth rate for the two higher values of α; for $\alpha = 20$, the observed rate is much lower. The stabilizing influence of nonlocal effects may help to explain the smaller variation of observed growth rates with respect to position. Even though the growth rate prediction is made for short wavelength local instabilities, it does seem to be a relatively good predictor of the overall stability of a vortex ring. Those with higher predicted growth rates have higher observed growth rates. Finally, notice that the rings become less stable as α increases.

Now we observe the time-dependent behavior of a one-parameter family of rings, where $\alpha = 50$ and $\beta = 0$, 20, 40. The case $\beta = 0$ is a ring with the Beltrami property, described in Section 2. They are computed with different mesh sizes but all contain approximately 3000–4000 representative particles in $\frac{1}{4}$ of the vortex ring. Specific information about each vortex ring is contained in Table IV. The relative velocity deviations for each ring are included in Table V, along with the predicted growth rates. The results for the ring with $\beta = 20$ were shown previously; the rest are graphed in Figs. 11 and 12.

TABLE IV

Information on a Family Varying in β

β	h	n	Prop. speed	$\psi_{\max}$	$T_{\min}$
0	0.09	4315	0.0543	0.102	11.3
20	0.08	4270	0.0671	0.103	7.76
40	0.08	3289	0.0752	0.104	5.92

While the growth rates, both observed and predicted, of these three rings vary much less across the family than previously, the predicted growth rates are still on the order of twice those observed. As before, the observed growth rates vary less across the level sets of ψ than the predicted growth rates. Here, however, the predicted growth rates do not always predict the relative stability. In particular, the ring with $\alpha = 50$ and $\beta = 20$ is predicted to have intermediate growth rates while some of its observed growth rates are lower than the other two. The rings in this family have such similar growth rates, however, that this is not surprising. In fact, increasing β does not seem to have a definitive influence on stability.

6. CONCLUSIONS

Axisymmetric rings with swirl have been computed as exact, steady solutions of the Euler equations of inviscid fluid flow, using a variational method. Quantitative predictions were made for the maximum growth rate of linearized, short-wave instabilities in these rings, using a geometric optics or WKB approach. A modified three-dimensional vortex method was developed to compute time-dependent perturbations in the exact rings for comparison with these predictions. Time-dependent calculations of unperturbed rings stayed close to the initial state for a moderate amount of time, at least for rings with certain choices of parameters. These calculations establish that the rings chosen are fairly

TABLE V

Growth Rates for a Family Varying in β

	$\beta = 0$		$\beta = 20$		$\beta = 40$	
Level	Predicted	Observed	Predicted	Observed	Predicted	Observed
1	0.264	0.141	0.338	0.148	0.394	0.150
2	0.291	0.142	0.370	0.153	0.425	0.153
3	0.308	0.157	0.387	0.155	0.437	0.156
4	0.317	0.154	0.396	0.151	0.438	0.158
5	0.319	0.166	0.396	0.151	0.420	0.163
6	0.314	0.160	0.384	0.151	0.387	0.168
7	0.302	0.150	0.351	0.147	0.347	0.167
8	0.276	0.132	0.292	0.137	0.308	0.156
9	0.225	0.115	0.199	0.119	0.255	0.134
10	0.139	0.102	0.111	0.076	0.130	0.097

stable and that they are represented with good accuracy by the vortex method. Finally, for each of five different exact rings, a general disturbance was introduced and allowed to evolve in time, using the modified vortex method. The growth rate was found, as a function of position in the ring, and compared with the maximum rate predicted by the WKB analysis. The observed rate of growth was about $\frac{1}{2}$ to $\frac{1}{3}$ of the predicted maximum, with the exception of the case $\alpha = 20$, $\beta = 20$. The dependence on location and on the ring parameters was generally consistent with the predictions, although there was less spatial variation in the observed rates than in the predicted ones.

These results indicate that the WKB analysis has done a reasonably good job of predicting the growth of instabilities. The fact that the predicted growth rates are larger than those observed can be explained by noting that the asymptotic analysis is predicting the maximum possible growth rate, while the vortex method calculation produces a rate for a particular disturbance not chosen to represent the maximum. It is also important to note that the WKB-type prediction excludes nonlocal interactions and assumes small wavelength perturbations, whereas the vortex method calculation includes the full effects but introduces a discretization error. Considering these limitations, the growth rate predictions seem to agree surprisingly well with those observed. This serves to increase our confidence in the performance of the modified vortex method as well as the asymptotic analysis. It also provides new information about the stability properties of the vortex rings with swirl, which we regard as a prototype for exact structures in inviscid flow.

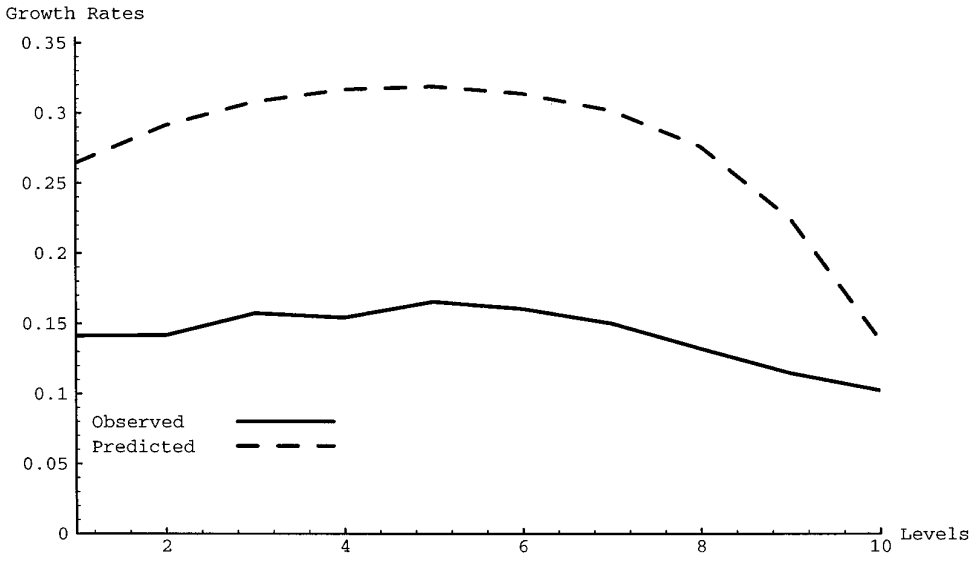

FIG. 11. Observed and predicted growth rates with $\alpha = 50$ and $\beta = 0$.

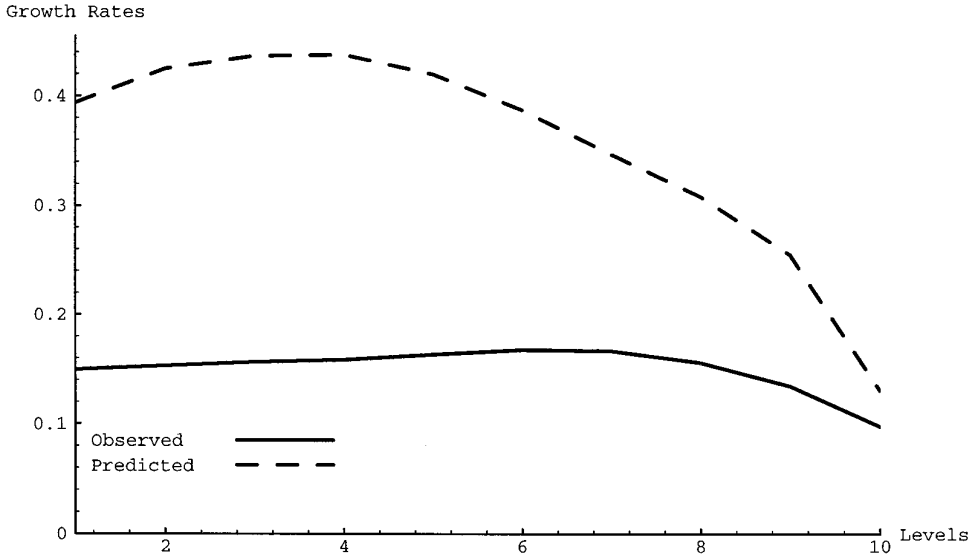

FIG. 12. Observed and predicted growth rates with $\alpha = 50$ and $\beta = 40$.

REFERENCES

1. C. Anderson and C. Greengard, On vortex methods, *SIAM J. Numer. Anal.* **22,** 413 (1985).
2. G. K. Batchelor, *An Introduction to Fluid Dynamics* (Cambridge Univ. Press, Cambridge, 1967).
3. B. Bayly, ''Computations of Broad-Band Instabilities in a Class of Closed-Streamline Flows,'' in *Mathematical Aspects of Vortex Dynamics*, edited by R. Caflisch (SIAM, Philadelphia, 1989), p. 50.
4. J. T. Beale, *Math. Comput.* **46,** 401, S15 (1986).
5. J. T. Beale, A. Eydeland, and B. Turkington, ''Numerical Test of 3-D Vortex Methods Using a Vortex Ring with Swirl,'' in *Vortex Dynamics and Vortex Methods*, edited by C. Anderson and C. Greengard, Lectures in Appl. Math, Vol. 28 (Am. Math. Soc., Providence, RI, 1991), p. 1.
6. J. T. Beale and A. Majda, *J. Comput. Phys.* **58,** 188 (1985).
7. T. Buttke, ''Fast Vortex Methods in Three Dimensions,'' in *Vortex Dynamics and Vortex Methods*, edited by C. Anderson and C. Greengard Lectures in Appl. Math, Vol. 28 (Am. Math. Soc., Providence, RI, 1991), p. 51.
8. A. J. Chorin, *SIAM J. Sci. Statist. Comput.* **1,** 1 (1980).
9. A. J. Chorin, *Commun. Math. Phys.* **83,** 517 (1982).
10. G. H. Cottet, *Ann. Inst. H. Poincaré* **5,** 227 (1988).
11. A. Eydeland and B. Turkington, *J. Comput. Phys.* **78,** 194 (1988).
12. A. Eydeland and B. Turkington, ''A Numerical Study of Vortex Rings with Swirl,'' in *GANG Report 12, Series I,* (Univ. Mass., Amherst, 1988).
13. L. E. Fraenkel and M. Berger, *Acta Math.* **132,** 13 (1974).
14. A. Friedman and B. Turkington, *Trans. Amer. Math. Soc.* **268,** 1 (1981).
15. L. Greengard, *The Rapid Evaluation of Potential Fields in Particle Systems* (MIT Press, Cambridge, 1988).
16. L. Greengard and V. Rokhlin, *J. Comput. Phys.* **2,** 325 (1987).
17. K. Gustafasson and J. Sethian (Eds.), *Vortex Methods and Vortex Motion* (SIAM, Philadelphia, 1991).
18. O. Knio and A. Ghoniem, *J. Comput. Phys.* **86,** 75 (1990).
19. A. Leonard, *J. Comput. Phys.* **37,** 289 (1980).
20. A. Leonard, *Annu. Rev. Fluid Mech.* **17,** 523 (1985).
21. A. Lifschitz, *Phys. Lett. A* **157,** 481 (1991).
22. A. Lifschitz, *Adv. Appl. Math.* **15,** 404 (1994).
23. A. Lifschitz and E. Hameiri, *Phys. Fluids A* **3,** 2644 (1991).
24. A. Lifschitz and E. Hameiri,*Commun. Pure Appl. Math.* **46,** 1379 (1993).
25. T. Lundgren and W. Ashurst, *J. Fluid Mech.* **200,** 283 (1989).
26. J. Martin and E. Meiburg, *J. Fluid Mech.* **230,** 271 (1991).
27. J. Martin and E. Meiburg, *J. Fluid Mech.* **243,** 457 (1992).
28. H. Moffatt, *J. Fluid Mech.* **35,** 117 (1969).
29. H. Moffatt, *J. Fluid Mech.* **173,** 289 (1986).
30. H. Moffatt, *Fluid Dyn. Res.* **3,** 22 (1988).
31. E. G. Puckett, ''Vortex Methods: An Introduction and Survey of Selected Research Topics,'' in *Incompressible Computational Fluid Dynamics*, edited by M. Gunzburger and R. Nicolaides (Cambridge Univ. Press, Cambridge, 1993), p. 335.
32. P. Saffman, *J. Fluid Mech.* **84,** 625 (1978).
33. P. Saffman, *Vortex Dynamics* (Cambridge Univ. Press, Cambridge, 1992).
34. K. Shariff and A. Leonard, *Annu. Rev. Fluid Mech.* **24,** 235 (1992).
35. K. Shariff, R. Verzicco, and P. Orlandi, *J. Fluid Mech.* **279,** 351 (1994).
36. W. H. Suters, Ph.D. thesis, Duke University, 1994.
37. B. Turkington, *SIAM J. Math. Anal.* **20,** 57 (1989).
38. B. Turkington and A. Eydeland, ''An Iterative Method for Computing Steady Vortex Flow Systems,'' in *Mathematical Aspects of Vortex Dynamics*, edited by R. Caflisch (SIAM, Philadelphia, 1989). p. 80.
39. S. Widnall, D. Bliss, and C.-Y. Tsai, *J. Fluid Mech.* **66,** 35 (1974).
40. S. Widnall and C.-Y. Tsai, *Philos. Trans. R. Soc. London Ser. A* **287,** 273 (1977).
41. G. Winckelmans and A. Leonard, ''Improved Vortex Methods for Three-Dimensional Flows,'' in *Mathematical Aspects of Vortex Dynamics*, edited by R. Caflisch (SIAM, Philadelphia, 1989), p. 25.